Scientific Research Publishing

International Journal of Geosciences, 2022, 13, 793-829
https://www.scirp.org/journal/ijg
ISSN Online: 2156-8367
ISSN Print: 2156-8359

Astronomical Triggers as a Cause of Strong Earthquakes

Alexander N. Safronov

Obukhov Institute of Atmospheric Physics, Russian Academy of Sciences/Pyzhevskii per. 3, Moscow, Russia
Email: safronov_2003@mail.ru

How to cite this paper: Safronov, A.N. (2022) Astronomical Triggers as a Cause of Strong Earthquakes. *International Journal of Geosciences*, **13**, 793-829.
https://doi.org/10.4236/ijg.2022.139040

Received: August 22, 2022
Accepted: September 26, 2022
Published: September 29, 2022

Abstract

The planetary geometries were studied at the moments of 92 strong earthquakes with a magnitude of more than 8 on the Richter scale (R8+) for the period from 1900 to 2011. Three main planetary schemes were specified, namely the schemes of the generalized Archimedes lever (gAL) and the Kepler conjunction (gKc), as well as a new geometry of the triangles of the remote signal catcher (cRS). It was discovered 22 gAL, 42 gKc and 28 cRS geometries, which are 23.9%, 45.7%, and 30.4%, respectively, from the total 92 studying cases. It was found that in some earthquakes; the planetary geometries are absolutely identical, which indicates the universality of the mechanism that caused the earthquake. The triggered effect does not depend on the distance between the planets and the mass of the planets, so the mechanism is identified as an inertial gravitational interaction. The triggered effect increases with the multiplicity of the ratio of distances between planets, as well as with pairwise planetary parallelism, which probably indicates about the wave nature of inertial effects. The triggering effect increases with increasing multiplicity of the ratio of distances between planets, as well as with pairwise planetary parallelism, which probably indicates about the wave nature of inertial effects. According to the Archimedes' lever principle, the Third Law of Motion is changed by adding a few words. It is assumed that inertia is a special case of gravity, namely gravitational self-induction, which really depends, like any self-induction, only on the geometry of the task.

Keywords

Earthquake, Planet Geometry, Ancient Seismology, Archimedes Lever, Kepler Conjunction, Third Law of Motion, Inertia, Gravity Wave

1. Introduction

The answer to the question: "Do planets have a significant impact on natural

processes or not?" has been worrying humanity for more than 2.5 thousand years. Undoubtedly, such a position should cause serious concerns. For those who did not know or prefer to forget, we remind the following historical aspects. In this study, as in the author's previous works, in order to avoid different interpretations of historical facts and texts in the oldest papyri, a reference to ancient seismology is given according to Archimedes. According to Pappus of Alexandria, Archimedes' levers were as follows (Archimedes, Syracuse, 287-212 BC):

"Give me a place to stand and with a lever I will move the whole world" (1)

Note that ancient seismology existed long before Archimedes, and it did not end with the works of Archimedes. Ancient seismological (seismoacoustic) stations were usually located at temples. Recall that the school of Pythagoras (570-490 BC) was at the Temple of the Muses. This school was located in Crotone, in southern Italy. The Temple of the Muses was built over a geological crack, and there is also a seismic tunnel in this temple. As is known from historical sources, two scholars escaped in this shaft during the attack on the Pythagorean School.

If we move further on a historical scale, we will remember that the Neo-Platonism conflict led to dramatic events. As is known, Hypatia, the daughter of the famous mathematician and astronomer Theon, lived in Alexandria in 350/370-415 AD. According to historical records, she taught mathematics and astronomy at the Academy of Neo-Platonism. One of her students failed the geometry exam, got angry at Hypatia, killed her and set fire to the world-famous library in Alexandria. Thus, we see that the lessons of Pythagoras on two-dimensional geometry are poorly learned and often cause an inadequate reaction. For convenience, the chronology of the conflict between supporters and opponents of the answer to the question is presented in **Table 1**.

Many years have passed since the destruction of the Pythagorean School and the burning of the Library in Alexandria. Another black date for ancient seismology and volcanology is the moment when the heathen temples were closed by the Roman Emperor Constantine I (272-337 AD). Since temples in remote provinces of the Roman Empire were closed last, it is highly likely that the seismological station at the Temple of Plutonium in Hierapolis, south-western Anatolia, was one of the last to be closed. The closure of this last seismic station occurred around 333 AD. A geological fault passed right under this Temple. The fault is active to the present, and the composition of volcanic gases is emitted through a seismological tunnel (called as Pluto Gate). Thus, a system of ancient seismic stations existed in the Mediterranean for ~550 years after Archimedes, who lived in 287-212 BC. Consequently, a system of seismic stations existed in the Mediterranean for at least ~200 years before Archimedes.

The selectivity of the knowledge of modern geophysicists and their unwillingness to recognize the works of ancient European philosophies, such as Pythagoras, Plato, Aristotle, and Archimedes, look extremely suspicious. In more details the historical aspects were discussed early in [1] [2] and some remarks

Table 1. The chronology of the conflict which extended more than 2.5 thousand years.

Answer for question:		
Whether linear configuration of planets have an essential impact on the natural processes or not?		
YES		NO
The Ancient World		
Mesopotamia priests Minor Asia priests Moses		Egyptian priests
The Hellenistic World		
Pythagoras Plato Aristotle Archimedes		Hebraic priests
Roman Republic and Empire		
Hypatia of Alexandria		Emperor Constantine I
Middle Ages		
Johannes Kepler Johann Elert Bode		Isaac Newton
The Present		
Geosciences:	Climatology Meteorology Seismology Volcanology Geodynamics	Albert Einstein LIGO/VIRGO Team Galaxy Evolution Teams
Astrophysics:	Solar physics Exoplanet astronomy Nuclear astrophysics	

about the modern Holy Inquisition can also be found in [3].

It should be noted that earlier the discussion of the possibility of predicting earthquakes caused a heated discussion. Detailed information about what earthquake can or cannot be predicted can be investigated by Tomaschek (1959), (Burr, (1960), Gribben, (1973-1076), Meeus, (1975), Bolt and Wang in (1975), Ip (1976), Hughes (1977), Geller (1997), Omerbashich (2012), Mörner with colleges (2013), Scafetta and Mazzarella, (2015), Marilia and Azevedo in 2017, Hagen and Azevedo in 2019, Awadh (2021), Safronov, (2022), please see [3]-[24]. In this paper, we will not dwell on this discussion, but will focus in detail on the analysis of the planetary geometry in strong earthquakes.

Note that the moment of the amount of motion (the vortex of inertial mo-

tion), can take on our planet, in addition to the lithosphere, as well as the atmosphere, hydrosphere and asthenosphere. Therefore, it is not surprising that with certain planetary geometries and the inclination of the Earth's axis, in addition to initiating earthquakes, changes in the Earth's rotation speed, vortex processes begin in the atmosphere, starting a volcanic eruption, as well as changes in the Earth's magnetic fields and generations of a low-frequency electromagnetic radiation can be generated. All these related processes are beyond the scope of this study.

On the other hand, the external momentum of the amount of motion can be perceived by other planets and the Sun, so this can lead to an impact on solar activity, in particular the formation of sunspots and the formation of solar prominences.

The fact that under certain conditions earthquakes are accompanied by side effects has been repeatedly investigated. For the planetary-solar-terrestrial interaction, and the correlation between earthquakes and the terrestrial rotation see chronology of studies: Bollinger (1952), Simpson (1968), Gribben (1971-1973), Wood (1972), Anderson (1974), Condon and Schmidt in 1975, Gu Zhen-Nian (1995), Zharov (1996), Soldati and Spada (1999), Han *et al.* (2004), Li (2006), Hung (2007), Odintsov *et al.* (2007), Scafetta (2010-2014), Tavares and Azevedo (2011), (Abreu *et al.*, (2012), Mörner and colleges (2013), Okhlopkov (2014), Stefani *et al.*, (2016, 2019), Marchitelli *et al.*, (2020), please see [6] [19] [20] and [25]-[45], and the works cited in them.

Due to the smallness of the gravitational constant, which leads to the smallness of tide interaction, the effects presented in the above works contradict the concept of Einstein's followers (**Table 1**). Therefore, these works are either ignored, or the journals in which these works are published have been closed. In particular, due to the publication of articles on planetary-solar-terrestrial interaction, which is a development of the Kepler's concept, the journal "*Pattern Recognition in Physics*" was closed. Researchers of the Titius-Bode law were also unlucky; Einstein's followers, who have settled in such journals as Nature and Icarus, strongly prevent the publication of articles on orbital resonance and exoplanet investigations. General information about the Titius-Bode law can be found, e.g. in [46]-[52] and many others.

In order not to complicate the description of the earthquake initialization process due to astronomical factors, as well as in order to distance ourselves from excessively heated discussions, we will limit ourselves to citing these works. The reader in above publications can get acquainted in detail with the state of affairs.

Thus, the goal of this study is to test the relationship between the planetary geometry and powerful earthquakes. Thus, in an ideological sense, this work is not original, since it is a reworking of the knowledge of the great ancient philosophers, astronomers and mathematicians. Let us inform the reader in advance that geometry in inertial physics turned out to be much more diverse and rich

than that of Pythagoras (the theory of musical strings), Archimedes (the theory of levers) or Kepler (the theory of planet conjunction). Of particular interest is the geometry of the planet configurations similar to a catcher, which is probably able to recognize external remote signals. In a sense, these catchers are similar to the interference schemes proposed in the eLISA experiment [53].

The study is of interest to geophysicists and astrophysicists, and in the historical aspects, it can probably be of interest to philosophers and historians of antiquity.

2. Materials and Methods

2.1. Strong Earthquakes as Studying Object

It is well known that earthquakes as well as tsunami, volcanic eruptions, and hurricanes are the cause of death of many people, for details please see statistics in the CRED International Disaster Database [54], CRED Report 2021 [55], and corresponded studies [56] [57] [58].

We used data from the United States Geological Survey (USGS), the Earthquake Hazards Program for 92 earthquakes with a magnitude greater than 8 points on the Richter scale that occurred between 1900 and 2011 [59]. These earthquakes are designed as R8+ earthquakes. The earthquake data are available from the USGS archive of the website [60] [61].

Powerful earthquakes are short-term events, although they are often accompanied by subsequent weaker aftershocks. The short duration of earthquakes, compared with the establishment of certain planetary configurations, gives us a unique opportunity to determine the angle of rotation of the planet at the time of the earthquake.

In this study, the concept of eUTC-line was introduced, that is, the direction in the plane of the solar system at the time of the earthquake. Accordingly, the polar UTC-axis is rotated so as the UTC-line corresponding to 12 UTC (noon) is always directed at the Sun.

2.2. Astronomical Data and Method

To investigate the causes of strong earthquakes, we need to measure astronomical angles and distances between planets. In this work, the Orbit Viewer java applet from Osamu and Ron was used [62], which was created by Osamu Ajiki (AstroArts Inc.) in 1996 and modified by Ron Baalke (NASA/Jet Propulsion Laboratory, below JPL) in 2000-2001.

The Original Orbit Viewer is an interactive applet that displays the orbits of small bodies, such as comets and asteroids in the solar system, in 3D projection. Orbits can be shown forward or backward. For example, visualization of comet 1P/Halley was presented in JPL Small-Body Database Browser [63]. For simplicity, all the figures below are presented in a 2D projection in the planetary plane. In this projection, the direction of rotation of the planet is counterclockwise. The applet Orbit Viewer (The Orbit Viewer application) has been adapted to meas-

ure the angles between the planets of the solar system and determine the proportions in the positions of the planets. The following abbreviations were used in this study: Mercury: Mr, Venus: V, Earth: E, Mars: M, Jupiter: J, Saturn: S, Uranus: U, Neptune: N.

The planets located along the line are designated as Planet1-Planet2-Planet3, in order of distance from the Sun. The calculation of the angle (in degrees) between the three planets was made when the vertex of an angle is placed on a more distant planet. For example, the angle for the linearity of J-E-V is the smaller angle between the two lines JE and JV. During our investigation of planetary geometry, the alignment angle between lines Planet$_i$-Planet$_j$ and Planet$_j$-Planet$_k$ was used; also please see Figure 1. This alignment angle α_{ijk} was defined in degrees as follows:

$$\alpha_{ijk} = 180^{\circ}/\pi \cdot \arccos\left(\left(R_{ij}^2 + R_{jk}^2 - R_{ik}^2\right)/\left(2 \cdot R_{ij} \cdot R_{jk}\right)\right) \quad (2)$$

where i, j, k, are the three planets of the Solar System; x_i, y_i, z_i, are the coordinates of the i-planet, and the distance between i and j planets is equal to $R_{ij} = \left(\left(x_i - x_j\right) + \left(y_i - y_j\right) + \left(z_i - z_j\right)\right)^{1/2}$.

Due to the fact that we are looking for tracer of interference, the spatial ratio designations as a ratio of distances between planets were used. The ratio of distances between the planets was designated as Planet$_i$-Planet$_j$/Planet$_n$-Planet$_m$. For example, the ratio of the distance between Saturn and Earth to the distance between Earth and Venus was labeled as SE/EV. Thus the ratio SE/EV was defined as:

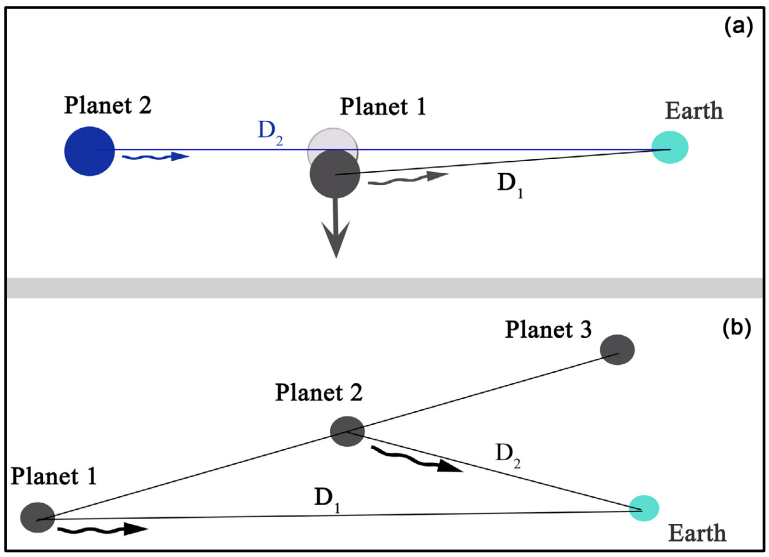

Figure 1. Two planetary alignment schemes are shown: (a) the linear scheme is marked in this study as L scheme. In history this scheme was called as the Archimedes' lever; (b) the triangular interference scheme is marked in this study as an X scheme. It is assumed that gravitational perturbations (vortexes) were created by the shading zones behind the planet in the solar system due to incomplete compensation. Maximum interference could be expected when the distances between planets D_1 and D_2 will be multiples.

$$N_{ij} = R_{53}/R_{32} \tag{3}$$

where R_{53} and R_{32} are a distances between Saturn and Venus to Earth. We are looking for the spatial ratio close to integer values.

Also in this study, the following symbols are introduced. The designation that the Planet$_i$-Planet$_j$ line is parallel to the Planet$_n$-Planet$_m$ line are marked as symbol "||", see Equation (4). Similarly, we highlight the fact that the line is perpendicular to another line, as symbol "⊥", see Equation (5). If the line crossing the position of Planet$_i$ it is drawn as symbol "→", see Equation (6):

$$\text{Planet}_i\text{Planet}_j \parallel \text{Planet}_n\text{Planet}_m \tag{4}$$

$$\text{Planet}_i\text{Planet}_j \perp \text{Planet}_n\text{Planet}_m \tag{5}$$

$$\text{line} \rightarrow \text{Planet}_i \tag{6}$$

3. The R8+ Earthquakes in Linear Planetary Configurations

3.1. The Archimedes Lever Planetary Alignments

Following the course of history, firstly, in this section we will consider the alignment of the planets without the participation of the Sun. Recall that before Copernicus, a geocentric model of the Solar System was used, so for scientists of the Ancient World, the Renaissance and the Middle Ages, only those alignments in which the Earth itself took part were available. Accordingly, the Earth is present in the formulation of the Archimedes' lever.

Two different planetary alignment schemes are shown in Figure 1. In history, the linear scheme, drawn in Figure 1(a) was called the Archimedes lever. In this study, the abbreviation for this type is L scheme. Linear alignment, in which the Earth does not participate in the alignment process, is shown in Figure 1(b). This triangular interference scheme is designated as an X scheme.

Twenty two cases have been found in which single or double alignments of planets take place. The Archimedes' lever planet alignments for R8+ earthquakes, *i.e.* with a magnitude greater than 8 on the Richter scale, are shown in Table 3. In this table, the studied cases are paired according to the planetary geometry. In the eighth column of Table 3, the planet geometry is briefly recorded. The symbols || and ⊥ mean parallelism and perpendicular between the line of the planet. The symbols used are described in Section 2.2. The ninth column of Table 3 presents the features of the eUTC-line. All Figures S1-S11, referenced in the second column of Table 3 can be found in the Supplementary. However, for convenience, several figures discussed below in text are duplicated and discussed in the main text of the manuscript.

3.2. The Kepler Conjunctions

In this section we present the results for the Sun-planet alignment schemes during R8+ earthquakes. Two Sun-planet alignment schemes were presented in Figure 2. The contiguous or opposite heliocentric alignment scheme, which is

Table 2. The Archimedes liner planet alignments at an angle of less than 0.5˚ for earthquakes with a magnitude of more than 8 points on the Richter scale (R8+). The studied cases are paired according to planetary alignments or earthquake locations.

ID	Figure	Position	R	Date, UTM	Planet alignment	Type	Planet parallelism	eUTC line
Archimedes lever alignments, 22 pcs								
1	1a	Kuril Islands	8.3	04.10.1994 13:22	J-V-E	L	-	They look the same.
2	1b	Kuril Islands	8.3	15.11.2006 11:14	J-V-E	L	-	
3	2a	Nankaido Japan	8.1	20.12.1946 19:19	J-V-E	L	-	They look the same.
4	2b	Hokkaido Japan	8.3	25.09.2003 19:50	J-E-M	L	-	
5	3a	Assam-Tibet	8.6	15.08.1950 14:09	M-Mr-V	X	-	→Mr
6	3b	Alaska	9.2	28.03.1964 3:36	M-Mr-V	X	-	→V
7	4a	Peru	8.4	23.06.2001 20:33	J-Mr-E-M	L	-	→V
8	4b	Colombia-Ecuador	8.8	31.01.1906 15:36	S-V-Mr	X	-	→M
9	5a	Bihar, India	8.1	15.01.1934 8:43	S-M-V-E	L	-	The β-angles are equal.
10	5b	central Mongolia	8.4	23.07.1905 2:46	J-M-V G-V-Sun	X, G	-	
11	6a	Shumagin, Alaska	8.2	10.11.1938 20:18	J-Mr-M S-E-M	L, X	-	The β-angles are equal.
12	6b	Macquarie Island	8.1	23.05.1989 10:54	J-V-E S-E-M	L, L	-	
13	7a	Solomon Islands	8	30.04.1939 2:55	J-V-Mr	X	MV || ESun	|| SunMr
14	7b	Solomon Islands	8	06.02.2013 01:12	J-Mr-V	X	-	→ Mr-M
15	8a	Valparaiso, Chile	8	03.03.1985 22:47	S-Mr-M	X	SJ || ME	|| VSun
16	8b	Papua, N.Guinea	8	16.11.2000 4:54	S-J-M	X	ESun || SM	|| SunMr
17	9a	Kuril Islands	8.2	07.09.1918 17:16	S-V-Mr-E G-Mr-Sun	L, X	SJ || SunE	⊥ SunV
18	9b	Okhotsk	8.3	24.05.2013 05:44	J-V-Mr	X	JM || VSun	-
19	10a	Loyalty Islands	8	20.09.1920 14:39	U-E-J U-M-S	L, X	SJ || SunE	→ Mr
20	10b	Northern Chile	8	30.07.1995 5:11	U-E-V	L	-	|| SJ
21	11a	Tonga region	8.2	30.04.1919 7:17	U-V-S	X	-	|| US
22	11b	southern Greece	8.3	11.08.1903 4:32	N-J-S	X	-	⊥ NS

drawn in Figure 2(a), is marked in this study as the Sun-L scheme. In history, this scheme was called the Kepler conjunction. Figure 2(b) shows a polar alignment scheme in which the Earth is excluded from the linear alignment process. This scheme is designated as the Sun-X scheme.

When studying 92 cases of R8+ earthquakes, 42 Kepler conjunctions were found. These Kepler conjunction schemes were presented in Table 3 and Table 4. The single Kepler conjunction cases were presented in Table 3. Table 4 records the results of the double Kepler conjunction schemes. The symbols used

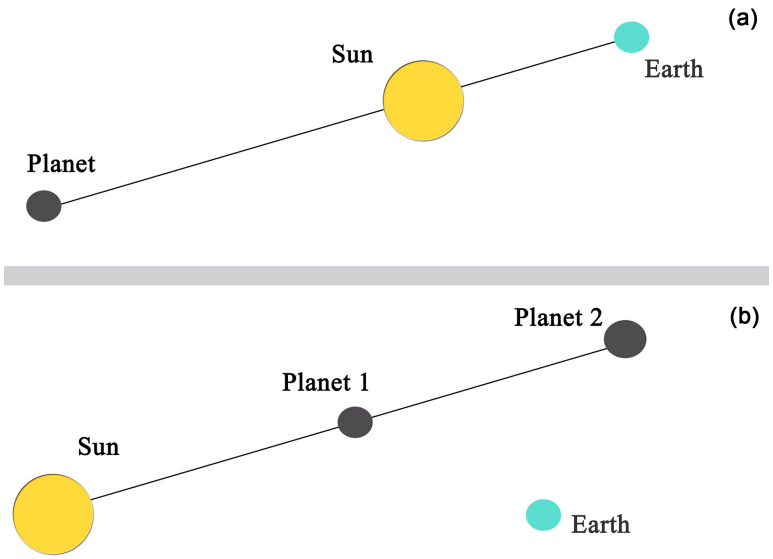

Figure 2. Two solar alignment schemes: (a) contiguous or opposite heliocentric alignment scheme, labeled as Sun-L. In history this scheme was called the Kepler conjunction; (b) another solar alignment scheme, in which the Earth is excluded from the linear alignment. In this study this scheme is named as the Sun-X scheme.

in Table 3 and Table 4 are similar to the symbols in the previous Table 3 and Table 4 are described in Section 2.2. All Figures of Kepler conjunctions are presented in Figures S12-S26 and S27-S32 in Supplementary.

Summarizing Section 3, we can draw the following conclusion. In general, strong earthquakes are triggered by gravitational processes during the alignment of the planet type (L, X) or solar type (Sun-L, Sun-X). Due to the fact that they do not depend on the distances between the planets and the masses of the planets, but are determined by the planet geometry, it is possible to draw a conclusion that earthquakes are initiated by the gravitational inertia processes.

4. The Catcher Schemes at the R8+ Earthquakes

In the previous section, the results related to the planet alignments or solar-planet conjunctions were presented. Previously these schemes have been studied to some extent, see, e.g. [3] [7] [19] [20] [64]. In this section we focus on the study of another aspect, namely the occurrence of resonant planetary configurations during the movement of planets. Planetary schemes that can be responsible for detecting both local gravitational disturbances and signals from remote sources have been designated as catcher Remote Signal (cRS) schemes. The simplest cRS scheme is shown in Figure 3(a). The interference maximum could be expected when the distances between the planets are multiple or equal.

Further, it is interesting to compare our cRS interference scheme with the geometric scheme of the evolved Laser Interferometer Space Antenna (eLISA). The eLISA scheme for determining gravitational waves should consist of three satellites located approximately in Earth orbit at the vertices of an equilateral

Table 3. The Kepler single conjunction studied cases with an angle of less than 0.5˚ for earthquakes with a magnitude greater than 8 on the Richter scale (R8+). The studied cases are paired in accordance with planetary alignments and/or the earthquake distribution.

ID	Figure	Position	R	Date, UTM	Planetary alignment	Type	Planet parallelism	eUTC line
Kepler single conjunction studying cases, 30 pcs								
23	12a	Sanriku, Japan	8.4	02.03.1933 17:31	M-E-Sun	Sun-L	-	The β-angles are equal
24	12b	Colombia	8	31.07.1970 17:08	M-Sun-E	Sun-L	-	
25	13a	Chile	9.5	22.05.1960 19:11	J-Sun-Mr	Sun-X	-	The β-angles are equal
26	13b	Iquique, Chile	8.2	01.04.2014 23:46	J-Sun-Mr	Sun-X	-	
27	14a	central Peru	8.2	24.08.1942 22:50	J-V-Sun	Sun-X	JM || VMr	The β-angles are equal
28	14b	central Peru	8.1	03.10.1974 14:21	J-Sun-V	Sun-X	JE || MrV	
29	15a	Hokkaido Japan	8.1	04.03.1952 1:22	J-Mr-Sun	Sun-X	SunE || EV	The β-angles are approx. equal.
30	15b	Honshu, Japan	8.2	16.05.1968 0:49	J-Mr-Sun	Sun-X	MMr || EV	
31	16a	Oaxaca Mexico	8	17.06.1928 3:19	S-Sun-V	Sun-X	-	The β-angles are equal.
32	16b	Tres Picos Mexico	8.2	08.09.2017 04:49	S-Sun-V	Sun-X	MV || SunE	
33	17a	Kurile Islands	8	01.05.1915 5:00	E-Sun-Mr	Sun-L	-	The β-angles are equal.
34	17b	Taiwan region	8	05.06.1920 4:21	M-Sun-V	Sun-X	-	
35	18a	Afghanistan	8	21.10.1907 4:23	J-Sun-Mr	Sun-X	JSun || EM	The β-angles are equal.
36	18b	Pakistan	8	27.11.1945 21:57	J-Sun-Mr	Sun-X	JM || VSun	
37	19a	Tonga	8.4	26.06.1917 5:49	Sun-M-J G-Mr-Sun	Sun-X, G	-	$\perp$ ESun
38	19b	Tonga region	8.1	22.06.1977 12:08	S-Sun-V	Sun-X	-	$\perp$ MMr
39	20a	Kermadec, N. Zealand	8	01.05.1917 18:26	Sun-V-J	Sun-X, G	JM || EMr	The β-angles are approx. equal.
40	20b	Mindanao, Philippines	8.3	14.04.1924 16:20	J-M-Sun	Sun-X	JE || MMr	
41	21a	Kuril Islands	8.3	06.11.1958 22:58	J-V-Sun	Sun-X	-	The β-angles are approx. equal.
42	21b	Kuril Islands	8.2	11.08.1969 21:27	S-V-Sun-Mr	Sun-X	-	
43	22a	Sumatra, Indonesia	9.1	26.12.2004 0:58	M-V-Sun	Sun-X	-	The β-angles are approx. equal.
44	22b	N. Sumatra, Indonesia	8.6	28.03.2005 16:09	E-Sun-V	Sun-L	-	
45	23a	central Peru	8.1	17.10.1966 21:41	J-Sun-Mr	Sun-X	-	Ones is the bisector of angle
46	23b	La Paz, Bolivia	8.2	09.06.1994 0:33	J-Mr-Sun	Sun-X	-	
47	24a	Kamchatka	9	04.11.1952 16:58	V-Mr-Sun	Sun-X	-	The β-angles are equal.
48	24b	Macquarie Island	8.1	23.12.2004 14:59	M-V-Sun	Sun-X	-	
49	25a	Valparaiso, Chile	8.2	17.08.1906 0:40	J-Sun-V	Sun-X	-	$\perp$ JM
50	25b	Balleny Islands	8.1	25.03.1998 3:12	S-M-Sun G-Sun-E	Sun-X, G	-	|| SunV
51	26a	Alaska	8	07.05.1986 22:47	J-Mr-Sun	Sun-X	ME || SunV	$\rightarrow$ Mr
52	26b	West N. Guinea	8	26.05.1914 14:22	J-Sun-V	Sun-X	JE || MrV	$\perp$ MV

Table 4. The Kepler double conjunction studied cases with an angle of less than 0.5˚ for earthquakes with a magnitude greater than 8 on the Richter scale (R8+). The studied cases are paired in accordance with planetary alignments and/or the earthquake allocations.

ID	Figure	Position	R	Date, UTM	Planetary alignment	Type	Planet parallelism	eUTC line
Kepler double conjunctions studying cases, 12 pcs								
53	27a	Tonga	8	04.01.1903 5:07	S-V-Sun J-Mr-Sun	Sun-X Sun-X	SJ || ESun	⊥ EMr
54	27b	Tonga	8	03.05.2006 15:26	J-E-Sun S-M-Sun	Sun-L Sun-X	SJ || EM	⊥ EV
55	28a	Mongolia	8.4	09.07.1905 9:40	S-V-Sun J-V-E	Sun-X, L	SJ || EMr	|| SunM
56	28b	Banda Sea	8.5	01.02.1938 19:04	E-Sun-V S-M-E	Sun-L, L	-	|| MV
57	29a	Tonankai, Japan	8.1	07.12.1944 4:35	Sun-Mr-V	Sun-X	-	⊥ MMr
58	29b	Honshu, Japan	9.1	11.03.2011 5:46	S-Sun-J S-M-V	Sun-X, X	-	⊥ ESun
59	30a	Unimak, Alaska	8.1	01.04.1946 12:28	J-Mr-Sun J-E-V	Sun-X, L	JM || MrV	⊥ EM
60	30b	Maule, Chile	8.8	27.02.2010 6:34	J-Sun-E J-V-M	Sun-L G, X	-	⊥ EV
61	31a	Okhotsk	8	11.06.1902 5:00	U-E-Sun U-V-M	Sun-L, X	-	⊥ EM
62	31b	Kamchatka	8.2	04.05.1959 7:15	U-M-Sun	Sun-X	-	⊥ JM
63	32a	Papua Indonesia	8.1	10.01.1971 7:17	S-Sun-J S-V-M	Sun-X, X	-	⊥ VMr
64	32b	central Peru	8	15.08.2007 23:40	E-V-Sun-Mr	Sun-L-X	-	→ E-Sun-Mr

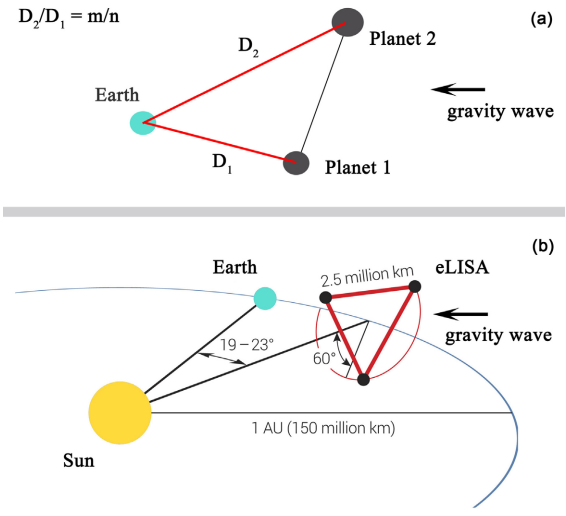

Figure 3. The triangular none linear alignment interference scheme is presented in (a). It is assumed that this triangular interference scheme is capable of registering signals from remote sources. The interference maximum could be expected when the distances between the planets D_1 and D_2 are multiples or equal. (b) shows for comparison a well-known isosceles triangle satellites scheme, which will be used in the future eLISA experiment by Baker *et al.* (2019) [69].

triangle at a distance of 2.5 × 106 km from each other. The satellite scheme that will be used in the future eLISA experiment is shown in Figure 3(b). Note that the launch of eLISA is expected in 2034. The scientific proposal for observations of gravitational waves in the millihertz band is well-summarized in [53] [65]-[70]. In this study, 28 cRS events were recorded in R8+ earthquakes. These results are presented in Table 5 and in the Supplementary.

Table 5. The catcher Remote Signal (cRS) studied cases of plane allocations with angle of less than 0.5˚ for earthquakes with the magnitude higher than 8 on the Richter scale (R8+). The studied cases are paired in accordance with the planetary alignments and/or the earthquake allocations.

ID	Figure	Position	R	Date, UTM	Galaxy impact	Planet parallelism	Major ratio	eUTC line
catcher Remote Signal (cRS) studying cases, 28 pcs								
65	33a	Jalisco, Mexico	8	09.10.1995 15:35	-	-	4.004	⊥ SM
66	33b	Lagunas, Peru	8	26.05.2019 07:41	-	-	5.950	⊥ SV
67	34a	Andrean Alaska	8.6	09.03.1957 14:22	-	-	0.998	⊥ SV
68	34b	northern Sumatra	8.6	11.04.2012 08:38	G-Sun-M	EV || MrSun	-	→ M
69	35a	Celebes Sea	8	15.08.1918 12:18	-	-	1.991	→ Sun
70	35b	Ndoi Island, Fiji	8.2	19.08.2018 00:19	G-Mr-Sun	VMr = EMr	-	→ Sun
71	36a	Sumatra, Indonesia	8.5	12.09.2007 11:10	G-V-Sun	MrSun || VM	2.970	⊥ SunMr
72	36a	Panay Philippines	8.2	24.01.1948 17:46	G-Mr-Sun	MSun || EMr	1.042	⊥ SunE
73	37a	Dominican Republic	8	04.08.1946 17:51	-	JE || MSun	6.015	-
74	37b	Jalisco, Mexico	8.1	03.06.1932 10:36	-	VMr || EM	5.997	-
75	38a	Chile-Argentina Border	8.5	11.11.1922 4:32	G-Sun-Mr	-	8.994	-
76	38b	Gobi-Altai, Mongolia	8.1	04.12.1957 3:37	-	-	11.044	-
77	39a	Solomon Islands	8.1	01.04.2007 20:39	-	JS || MSun	4.013	⊥ EV
78	39b	Samoa Islands	8.1	29.09.2009 17:48	-	SunMr || VM	3.038	⊥ SunE
79	40a	Kamchatka	8.5	03.02.1923 16:01	G-Sun-V	-	0.991	|| VMr
80	40b	Irian Jaya, Indonesia	8.2	17.02.1996 5:59	-	-	0.966	⊥ ESun
81	41a	Ecuador	8.1	12.12.1979 7:59	G-Sun-Mr	MMr || EV	1.023	⊥ MMr
82	41b	Michoacan, Mexico	8	19.09.1985 13:17	G-E-Sun	MSun || EV	1.018	⊥ VSun
83	42a	St. Vincent Azores	8.2	25.11.1941 18:03	G-Sun-Mr	SJ || MMr	1.984	⊥ ESun
84	42b	Mindanao Philippines	8	16.08.1976 16:11	G-Sun-V	JS || EV	2.022	|| VM
85	43a	Coquimbo, Chile	8.2	06.04.1943 16:07	G-Sun-N	SunV || MMr	0.986	-
86	43b	Sumbawa, Indonesia	8.3	19.08.1977 6:08	-	VE || SunMr	-	|| MrM
87	44a	Kuril Islands	8.5	13.10.1963 5:17	-	MV = VMr		|| VM
88	44b	Xinjiang, China	8	10.08.1931 21:18	-	-	1.994	⊥ EM
89	45a	Peru	8.2	12.12.1908 12:08	G-Sun-V	SJ || SunV	7.005	⊥ SJ
90	45b	central Peru	8.2	24.05.1940 16:33	-	SM || JSun	2.031	⊥ SE
91	46a	Ryukyu Islands	8.1	15.06.1911 14:26	G-Mr-Sun	VMr = EMr	-	⊥ SunV
92	46b	Alaska	8.7	04.02.1965 5:01	-	MV || ESun	3.025	⊥ EV

5. The Geometry of Archimedes Levers

As can be seen from Tables 2-5, nature is more diverse than previous researchers had assumed. The number and variety of geometric configurations in R8+ earthquakes are amazing. Due to the limited space, we can not write in the text about all these planetary configurations, so we will focus only on some of them in more detail.

Two planet geometries during strong R8+ earthquakes on the Kuril Islands, which occurred in 1994 and 2006, are shown in Figure 4(a) and Figure 4(b). These earthquakes occurred on the same alignments of Jupiter-Venus-Earth (J-V-E); please see the black lines in Figure 4. The 24-hours polar eUTC-axis is presented additionally. The other eUTC-axis, which corresponds to the UTC none position (12 UTC), represents the direction to the Sun. The terrestrial

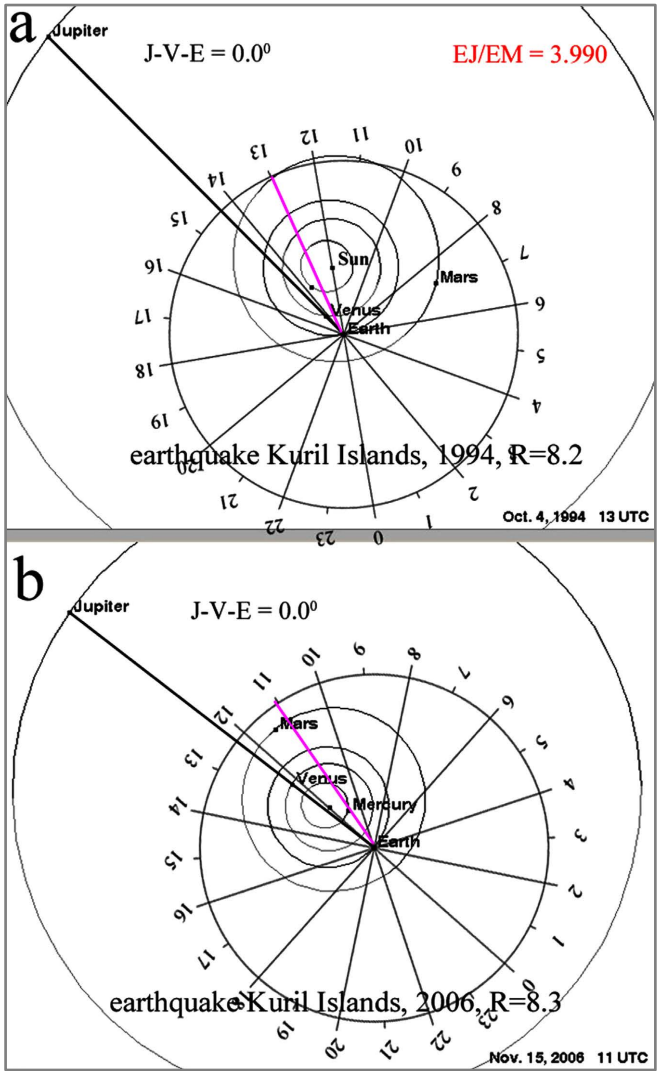

Figure 4. Two cases of strong earthquakes on the Kuril Islands in 1994 (a) and in 2006 (b) with the Jupiter-Venus-Earth alignments (black lines). The 24-hours polar eUTC-axis is presented additionally. The margin line is the terrestrial earthquake UTC location (eUTC-line), in which the position of noon UTC (12 UTC) is the direction to the Sun.

earthquake UTC time is presented by margin line (UTC-line). For ease of use and clarity, the eUTC-axes are not drawn in the figures below. It is assumed that the integer ratio in planet distance as well as planet parallelism are intensifying factor in gravity interferences. Thus, the ratio in this study is also the object of the investigation. The ratio is represented by red lines and/or red labels. The planetary geometry for these earthquakes is the same, but the ratios of EJ/EM are different.

Strong earthquakes often occur in the area along the Kamchatka-Hokkaido Geological Fault. The question arises: do all strong earthquakes in a given area always occur with this configuration as shown in Figure 4(a) and Figure 4(b)? Unfortunately, the answer is "*no*", nature is multifaceted.

The following planetary geometries during two strong earthquakes in Japan, which occurred in Nankaido in 1946 and in Hokkaido in 2003, are shown in Figure 5(a) and Figure 5(b). These two earthquakes also look the same, but

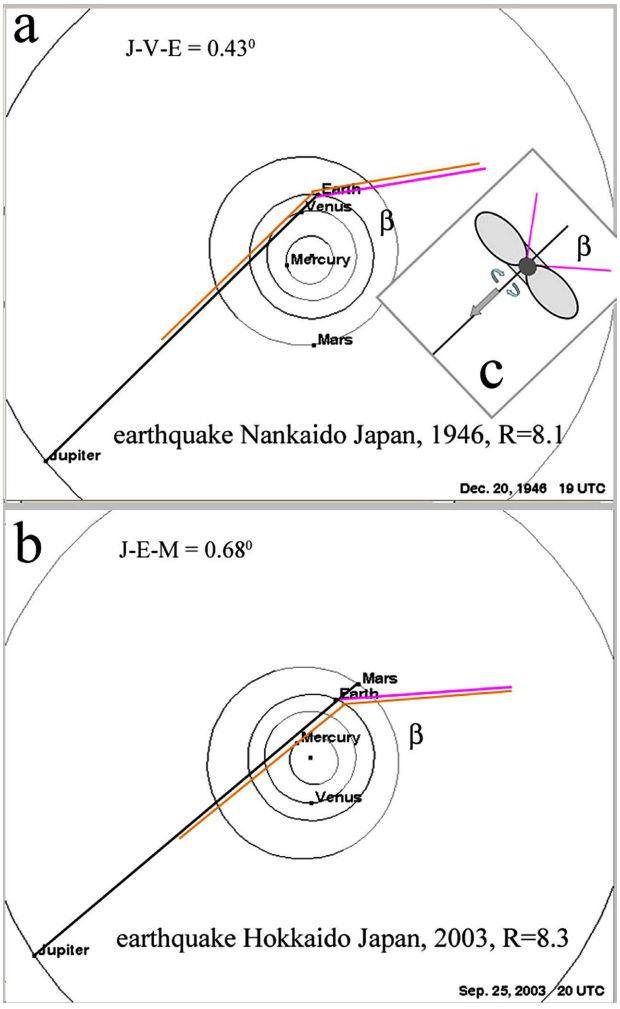

Figure 5. Similar planetary alignments have been drawn that took place during two earthquakes in Japan in Nankaido in 1946 (a) and Hokkaido in 2003 (b). The margin line is the terrestrial earthquake UTC line (eUTC-line). The proposed self-induction of an inertial as a torus-solution is shown in Figure (c).

their geometry differs from the one shown above in Figure 4.

Please note that the Nankaido earthquake (1946) occurred during the J-V-E alignment, whereas the Hokkaido earthquake (2003) occurred on the J-E-M alignment. Thus, the planets involved in the alignments in Figure 5 are different, and in Figure 5(b), during the Hokkaido earthquake, the Earth is located between Jupiter and Mars. In addition, the angles between the alignment line (black line) and the eUTC-line (margin line) are equal. Since the standard inertia solution is a torus or solenoid, we assume that in Figure 5(c) the eUTC-line is tangent to the inner circle of the inertial torus in L-schemes.

Then the following question arises: what will be the geometry of the interaction if the Earth is not involved in the alignment process? The planetary geometries of the X-schemes are demonstrated in Figure 6(a) and Figure 6(b) during

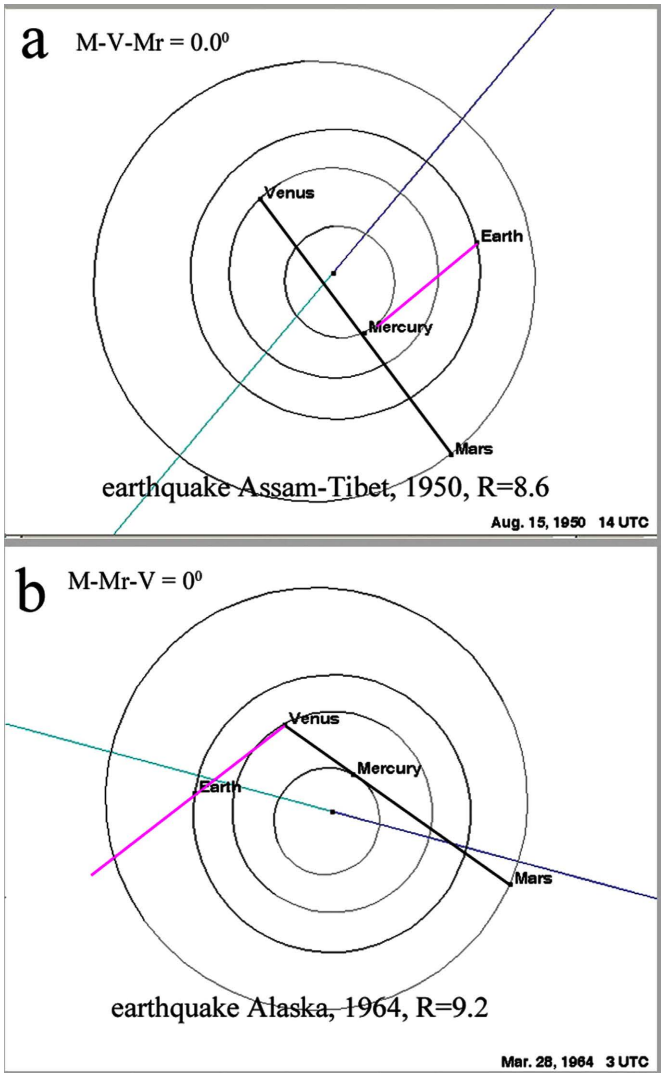

Figure 6. Planetary alignments are shown for earthquakes in Assam-Tibet, 1950 (a) and Alaska, 1964 (b). The axis of the galaxy was drawn by blue-green colors; these colors correspond to the center-anticenter directions. The eUTC-lines intersect the positions of Mercury (a) and Venus (b).

earthquakes that occurred in Assam-Tibet (1950) and Alaska (1964). As can be seen from Figure 6, the eUTC-lines cross the positions of Mercury (Figure 6(a)) and Venus (Figure 6(b)).

Figure 7 shows the long distant planetary alignments, in which the remote Uranium and Neptune were involved. These geometries correspond to the earthquakes in Loyalty Islands in 1920 (Figure 7(a)) and in southern Greece in 1903 (Figure 7(b)). In Figure 7(a), the eUTC-line is parallel to the Uranus-Venus-Saturn line, and in Figure 7(b), the line is perpendicular to the Neptune-Saturn-Jupiter line. Thus, the source of gravitational waves can be one planet, as shown in Figure 6, as well as a fully aligned line in the form of a "music string" of Pythagoras, as shown in Figure 7. Moreover, from the examples shown in Figure 7, it can be concluded that a gravitational wave can have two polarizations parallel to and perpendicular to the linear source.

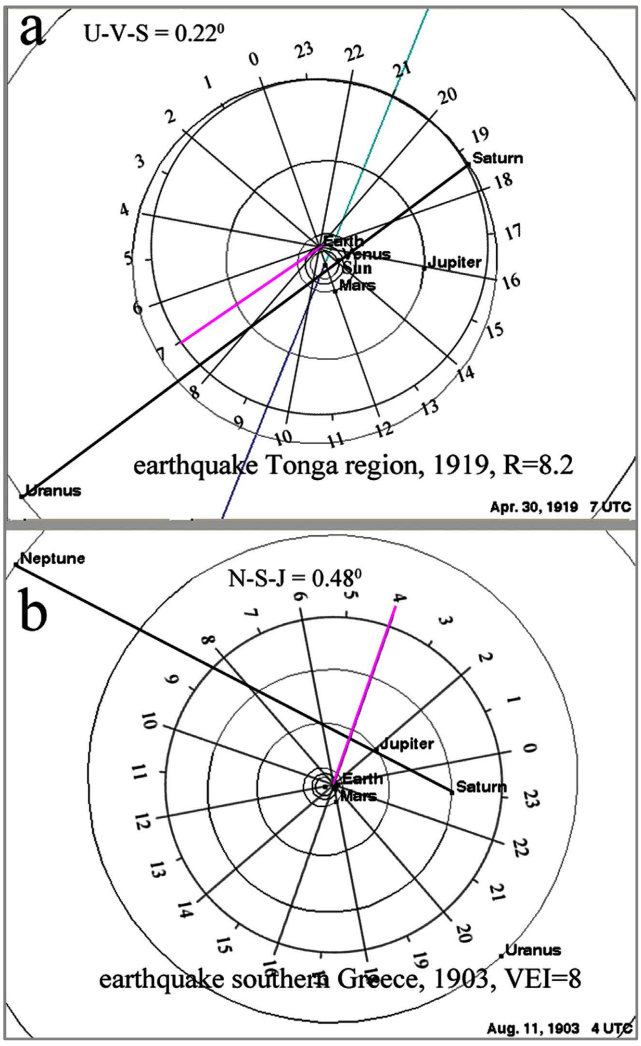

Figure 7. The longest planetary alignments involving the distant Saturn, Uranus and Neptune are shown for earthquakes on the Loyal Islands in 1920 (a) and in southern Greece in 1903 (b). In Figure (a), the eUTC-line is parallel to the Uranus-Venus-Saturn line, and in Figure (b) is perpendicular to Neptune-Saturn-Jupiter line.

6. The Geometry of Kepler Conjunctions

In this section, we will look at the geometry of Kepler conjunctions at the R8+ earthquakes. In Figure 8(a) and Figure 8(b) show two cases corresponding to the Sun-L scheme. These events correlate with the Mars-Earth-Sun alignment (Figure 8(a)) and Mars-Sun-Earth alignment (Figure 8(b)). Note that in these studied cases, Earth and Mars are located on the opposite side of the Sun. The margin line is the terrestrial earthquake UTC location (eUTC-line). The β-angles between the planetary alignments (black line) and the eUTC-line (margin line) are equal. These cases (Sun-L) have some analog with the geometry in Figures 4-6, which demonstrate the L-type of planetary alignments.

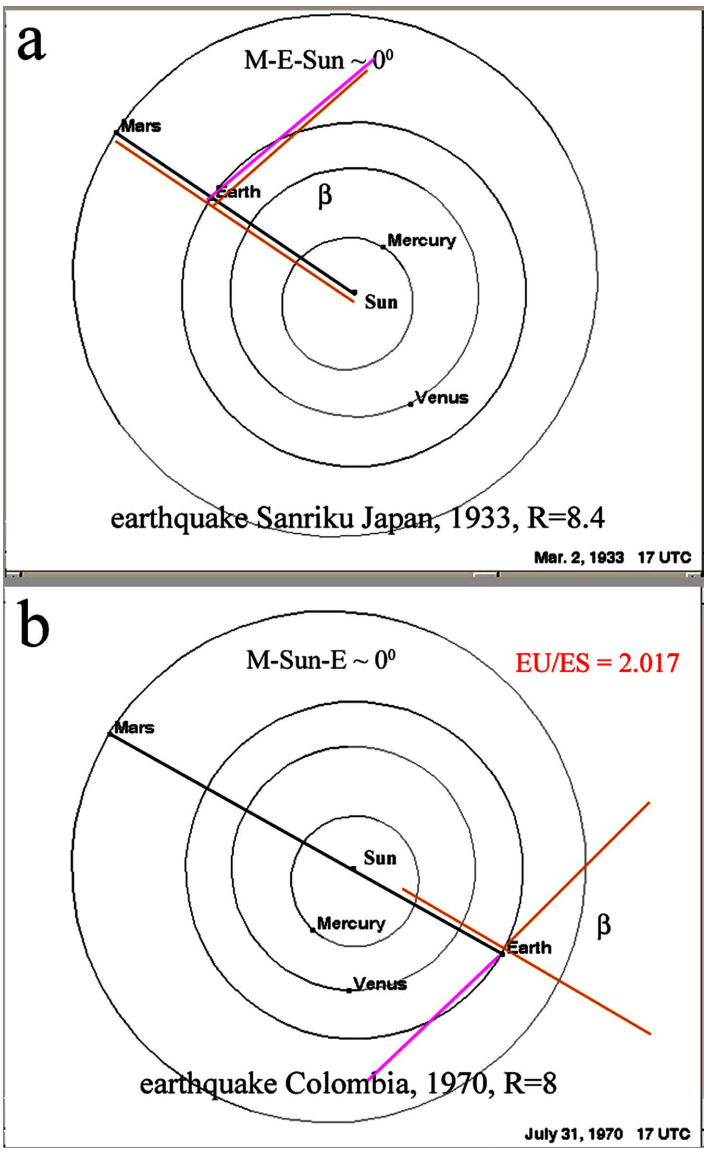

Figure 8. Two cases of Kepler's conjunction with Mars-Earth-Sun (a) and Mars-Sun-Earth (b) are presented. Earth and Mars are located on the opposite sides of the Sun. The margin line is the terrestrial earthquake UTC location. The β-angles between the planetary alignments (black line) and the eUTC-line (margin line) are equal.

Figure 9 shows several cases corresponding to the following Sun-X scheme, in which the Earth does not participate in the conjunctions. These earthquakes that occurred in Valparaiso (Chile) in 1906 (Figure 9(a)) and on the Balleny Islands in 1998 (Figure 9(b)) are presented. The Balleny Islands are a series of uninhabited islands in the Southern Ocean in southern Australia with coordinates (66.92˚S 163.75˚E). In Figure 9(a), the eUTC-line is perpendicular to the Jupiter-Mars line, and in Figure 9(b), the eUTC-line is parallel to the Sun-Venus line. Red lines and red marks indicated the resonance distance ratio. The interference maximum could be expected when the distances between the planets D_1 and D_2 are multiples.

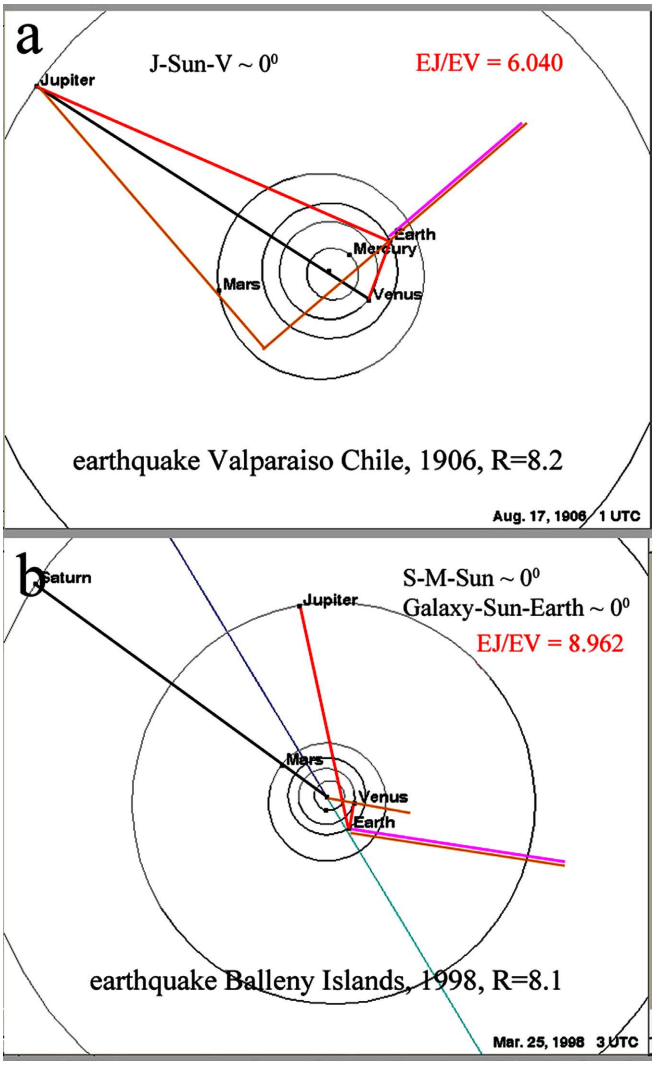

Figure 9. Two cases of studying the Kepler conjunction with strong earthquakes in Valparaiso (Chile) in 1906 (a) and on the Balleny Islands in 1998 (b) are presented. The Balleny Islands are a series of uninhabited islands in the Southern Ocean in southern Australia with coordinates (66.92˚S 163.75˚E). Red lines and red marks indicate the resonance distance ratio. The margin line is the terrestrial earthquake UTC location (eUTC-line). In Figure (a), the eUTC-line is perpendicular to the Jupiter-Mars line, and in Figure (b), the eUTC-line is parallel to the Sun-Venus line.

7. The Influence of Parallelism in Kepler Conjunction Schemes

In this study, it was discovered for the first time that pairwise parallelism of the distribution of planets is a frequent phenomenon in strong earthquakes. Figure 10 shows two such studied cases of strong earthquakes in Alaska (1986) and in West Guinea (1914). The blue lines and labels highlight the parallelism in this geometry. During the earthquake in Alaska (1986), the Mars-Earth line was parallel to the Sun-Venus line (Figure 10(a)), and during the earthquake in Guinea (1914), the Jupiter-Earth line was parallel to the Mercury-Venus line. In Figure 10(a), the continuation of the eUTC-line crosses Mercury position, and in Figure 10(b) the eUTC-line crosses nearby Venus position.

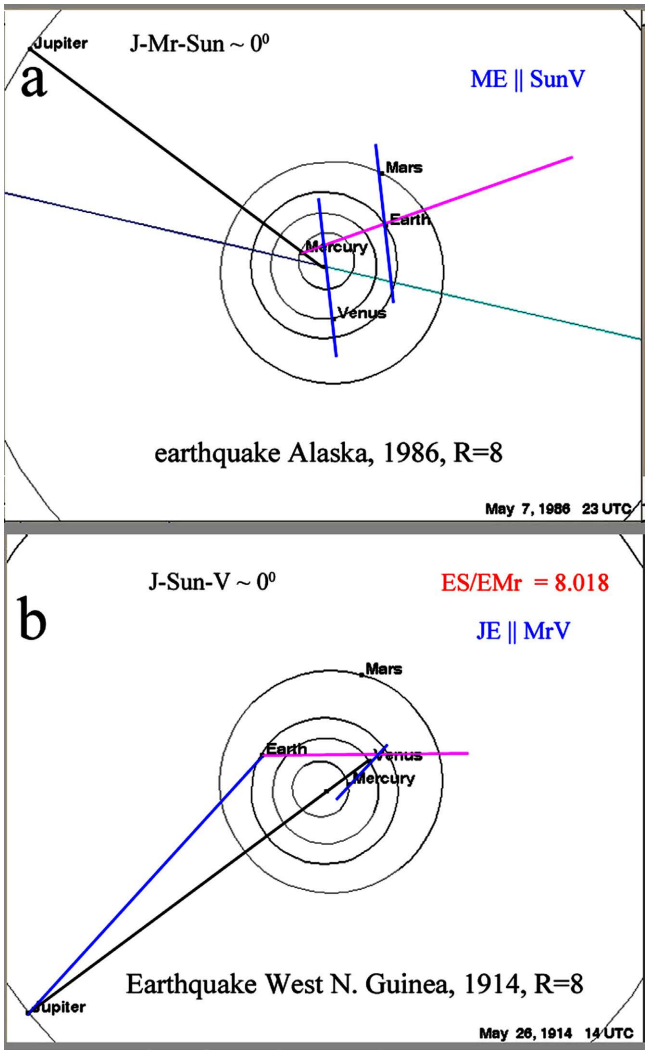

Figure 10. Two studied cases of strong earthquakes in Alaska in 1986 (a) and in the Western part of Northern Guinea in 1914 (b) are presented. Red lines and red marks denoted the resonance distance ratio. The margin line is the terrestrial earthquake UTC location (eUTC-line). In Figure (a) the continuation of the eUTC-line crosses a Mercury position, and in Figure (b) the eUTC-line crosses nearby Venus position. The blue lines and labels highlight the parallelism.

In addition, the double solar-planet alignments with paired planetary parallelisms was demonstrated during two earthquakes in Tonga in 1903 and 2003, see Figure 11(a) and Figure 11(b). The blue lines in Figures highlight the parallelism. In the Tonga earthquake (1903), the double conjunctions include the Saturn-Venus-Sun and Jupiter-Mercury-Sun lines, and in the Tonga earthquake (2003) the Saturn-Mars-Sun and Jupiter-Earth-Sun lines. In the Tonga earthquake (1903), the Saturn-Jupiter line was parallel to the Earth-Sun line, and in the Tonga earthquake (2003), the Saturn-Jupiter line was parallel to the Mars-Earth line. Further in Figure 11(a), the eUTC-line is perpendicular to the Earth-Mercury line, and in Figure 11(b) it is perpendicular to the Earth-Venus line.

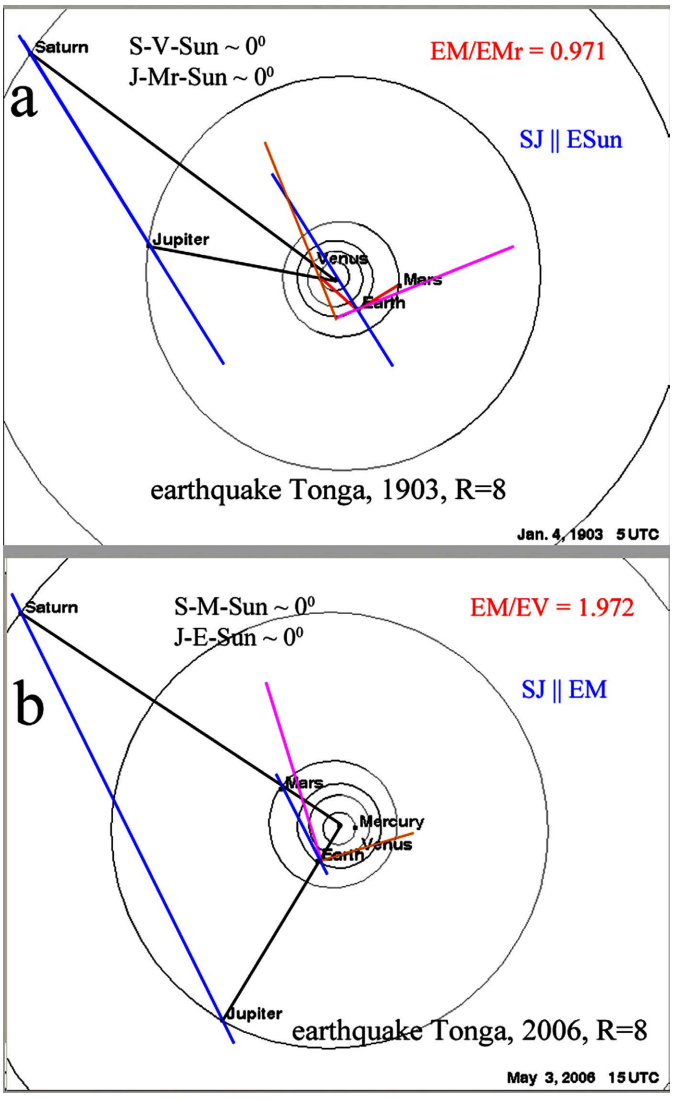

Figure 11. Double Kepler conjunctions have been demonstrated for two earthquakes in Tonga in 1903 (a) and 2003 (b). The margin eUTC-line is the terrestrial earthquake UTC location. The eUTC-line is perpendicular to the Earth-Mercury line in Figure (a) and perpendicular to the Earth-Venus line in Figure (b). Parallelism is highlighted with blue lines.

It is hard to imagine that such complex geometric patterns are a mere coincidence. It can be seen that in reality the inertial geometry of Kepler conjunction is much more complicated than the simplest scheme shown in Figure 2.

8. Geometry of the Catcher Remote Signal Events

Figure 3 above shows the general scheme of catcher Remote Signal (cRS) events. In this section, we will look at how such schemes are implemented in practice.

The cRS geometries are demonstrated by the example of the earthquakes in the Celebes Sea (1918) and on Odin Island, Fiji (2018) in Figure 12(a) and Figure 12(b). The resonance distance ratios occur between Mercury, Venus, and Earth. The margin lines in the Figures correspond to the terrestrial earthquake hour lines (eUTC-lines). The eUTC-line in Figure 12(a) is a bisector of the angle between Mercury, Earth and Venus. This bisector line crosses the position of the Sun. In other studied case, which is presented in Figure 12(b), the prolongation of the eUTM-line crosses the position of the Sun.

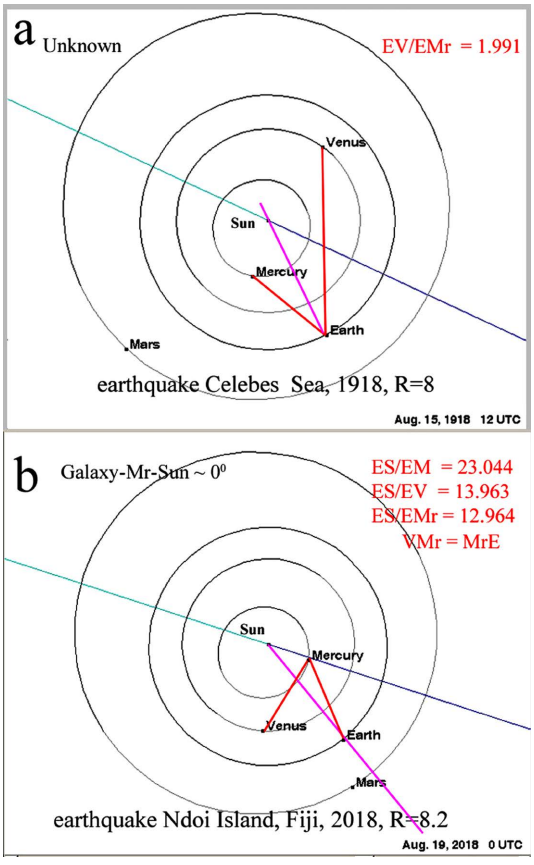

Figure 12. The planetary configurations were presented for the earthquake in the Celebes Sea in 1918 and on the Ndoi Island (Fiji) in 2018 (b). The resonance distance ratios between Mercury, Venus and Earth were presented by red lines and labels. The margin line corresponds to the terrestrial earthquake hour line (eUTC-line). The eUTC-line in Figure (a) is a bisector of the angle between Mercury, Earth and Venus. This bisector line in Figure (a) crosses the position of the Sun. In Figure (b), the prolongation of the eUTM-line crosses the position of the Sun.

Another example of the cRS geometries is shown in Figure 13. These planetary geometries are associated with two strong earthquakes that occurred in Kamchatka in 1923 and on Irian Jaya, Indonesia, in 1996. The resonance has in the distance ratios between Mercury, Venus and the Earth, in the Figures it is highlighted with red lines and labels. In Figure 13(a), the eUTM-line (margin line) is parallel to the Venus-Mercury line. In Figure 13(b), the perpendicular line to the eUTC-line is the bisector of the angle between Mercury, Earth and Venus with an additional cross transverse position of the Sun.

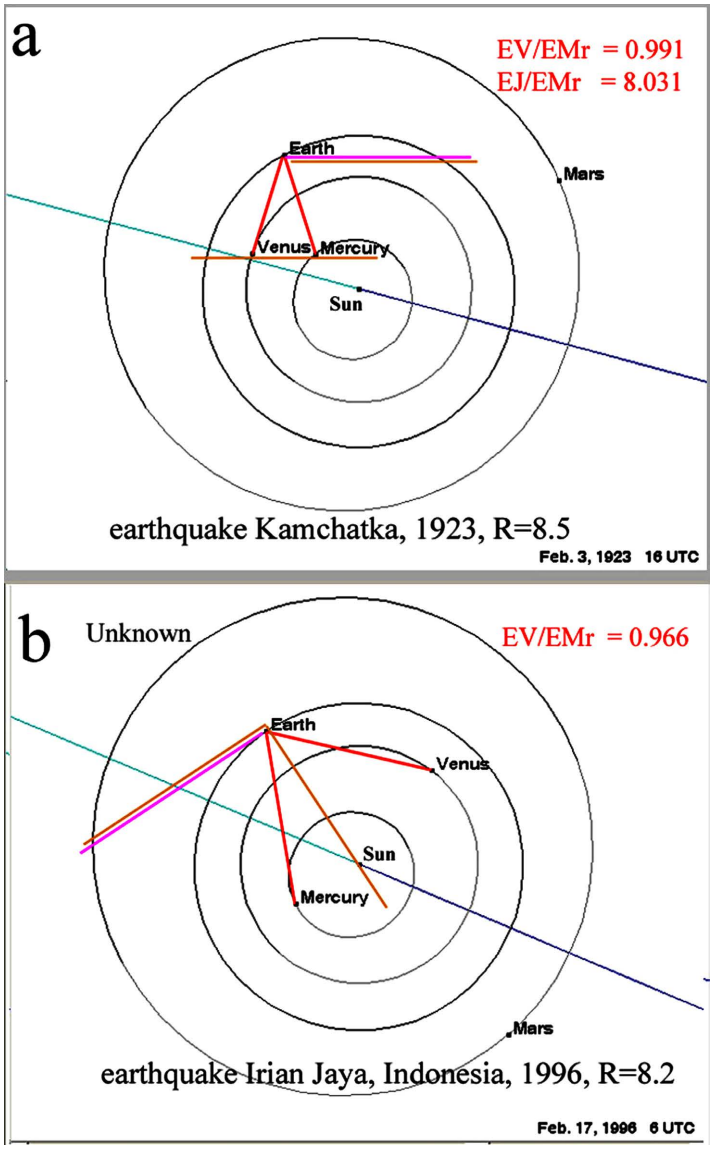

Figure 13. Planetary configurations were presented for strong earthquakes that occurred in Kamchatka in 1923 (a) and on Irian Jaya, Indonesia, in 1996. The resonance distance ratios between Mercury, Venus and Earth were presented by red lines and labels. The margin line corresponds to to the terrestrial earthquake hour line (eUTC-line). In Figure (a), the eUTM-line is parallel to the Venus-Mercury line. In Figure (b), the perpendicular to the eUTC-line is the bisector of the angle between Mercury, Earth and Venus with additional cross position of the Sun.

Finally, in Figure 14 we presented two unusual cRS schemes without a triangle. The planetary geometries, which took place in northern Sumatra (2012), and in Sumbawa, Indonesia (1977) are shown in Figure 14(a) and Figure 14(b). The resonance ratio is highlighted with red marks and lines. The margin line is the eUTC-line of the terrestrial earthquake UTC time. In these cases, (a) eUTC-line correlates with 9 UTC and with 6 UTC in (b), in which the earthquakes approximately occurred. In both cases, the Earth-Venus line is parallel to the Mercury-Sun line. The blue lines are drawn to highlight the planetary pairwise

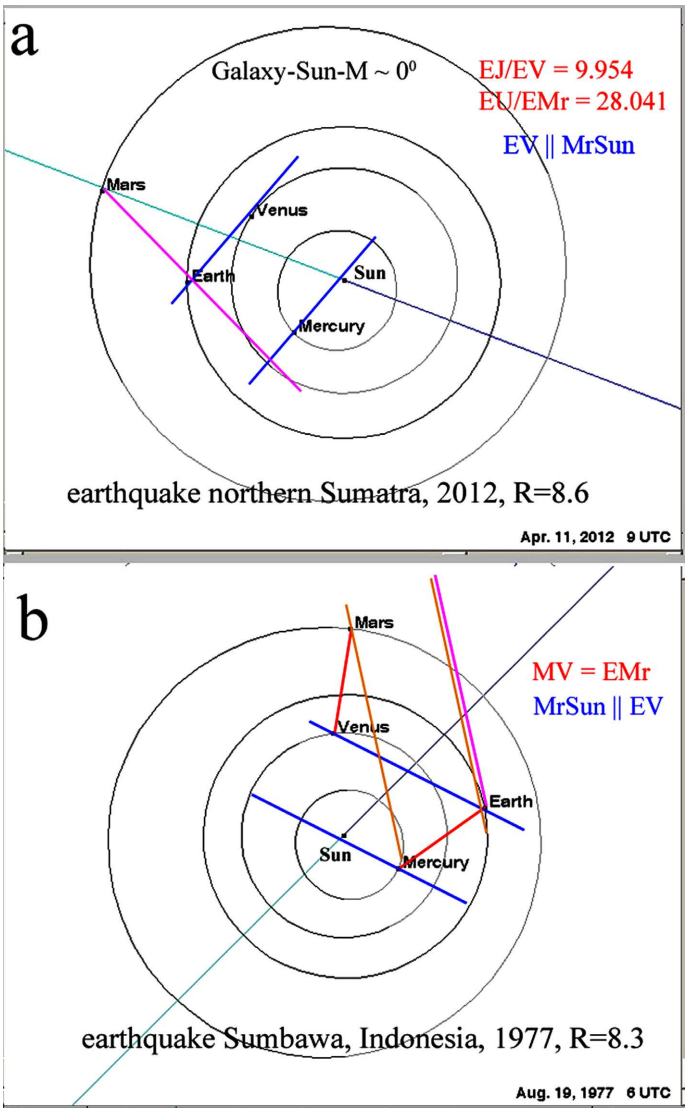

Figure 14. The planetary configurations for strong earthquakes that occurred in northern Sumatra in 2012 (a) and in Sumbawa, Indonesia in 1977 (b) are presented. The resonance ratio is highlighted with red marks and lines. The margin line is the eUTC-line of the terrestrial earthquake UTC time. In these cases, (a) eUTC-line correlates with 9 UTC and with 6 UTC in (b), in which the earthquakes approximately occurred. The dark blue lines are drawn the parallel planet lines. The eUTC-line at 9 o'clock UTC in Figure 15(a) indicates that Mars is probably involved in a resonance scheme. In Figure (b), the eUTM-line is parallel to the Mercury-Mars line.

parallelism. The prorogated of the eUTC-line at 9 o'clock UTC in Figure 14(a) indicates that Mars is probably involved in a resonance scheme. In Figure 14(b), the eUTM-line is parallel to the Mercury-Venus line. Considering these schemes, one can only wonder at the variety of manifestations of inertial interference. Other examples of more complex cRS schemes can be found in the Supplementary.

9. Summary Statistics

The R8+ statistic for 22 events of Archimedes lever alignments are summarized in Table 7. Note that the participation of Venus, Earth, Mars, Jupiter, and Saturn in the Archimedes lever is approximately the same and equal to ~10% - 15% (Table 6). Pairwise planetary parallelism is presented in the Archimedes

Table 6. The R8+ earthquake statistic for the Archimedes lever planetary alignments.

Archimedes lever study cases, 22 pcs.			Quantity	
			pcs	%
1	L	Linear alignment with Earth	12	54.5
2	X	Linear alignment without Earth	14	63.6
		Total amount including double alignments	26	118.2
Archimedes level scheme including			**Quantity**	
			pcs	**%**
1		Mercury	9	40.9
2		Venus	15	68.2
3		Earth	12	54.5
4		Mars	10	45.5
5		Jupiter	13	59.1
6		Saturn	10	45.5
7		Uranus	4	18.2
8		Neptune	1	4.5
Parallelism in the Archimedes level schemes			**Quantity**	
			pcs	**%**
1		Sun involved in the planet parallelism	5	22.7
2		Earth involved in the planet parallelism	5	22.7
		Total amount including multi parallelism	6	27.3
The eUTC-line features in the Archimedes levels			**Quantity**	
			pcs	**%**
1		The schemes are look similar	4	18.2
2		The β-angles are equal	4	18.2
3		The eUTC-line crosses the planet position	6	27.3
4		The eUTC-line is parallelized with planet line	5	22.7
5		The eUTC-line is perpendicular with planet line	2	9.1
6		The eUTC-line is unknown	1	4.5

level schemes, but it is not the dominant process. Then the double alignment events occur, but their number is not significant either.

Summary statistics for 42 Kepler conjunctions are presented in Table 7. Note that the number of Kepler conjunctions without Earth (Sun-X) is in 4 times greater than the number of cases of Kepler conjunctions with Earth (Sun-L). Further, in contrast to the planet alignments described in Section 3.1, in the solar-planet alignments the impact of Jupiter is dominant. The participation of Jupiter was recorded in 23 cases (54.8%); for comparison, the Earth was involved in only 8 cases (19.0%), see Table 7. Once again, we recall that the fierce debate about the "*Jupiter effect*" and "Kepler conjunction" was provoked by Gribben (1973) and then continued by Mörner and colleges [19]. For details of the "*Jupiter effect*", also please see [3], and the references provided in it.

Table 7. The R8+ earthquake statistic of Kepler conjunctions.

Kepler conjunctions, 42 pcs.			Quantity	
			pcs	%
1	Sun-L	Linear alignment with Earth	9	21.4
2	Sun-X	Linear alignment without Earth	36	85.7
	Total amount including double alignments		45	107.1
Kepler conjunctions including			**Quantity**	
			pcs	**%**
1	Sun		42	100
2	Mercury		16	38.1
3	Venus		20	47.6
4	Earth		8	19.0
5	Mars		9	21.4
6	Jupiter		23	54.8
7	Saturn		10	23.8
9	Uranium		2	4.8
Parallelism in the Kepler conjunction schemes			**Quantity**	
			pcs	**%**
1	Sun involved in the planet parallelism		6	14.3
2	Earth involved in the planet parallelism		9	21.4
	Total amount including multi parallelism		15	35.7
The eUTC-line features in the Kepler conjunctions			**Quantity**	
			pcs	**%**
1	The β-angles are equal		14	33.3
2	The β-angles are approx. equal		8	19.0
3	The eUTC-line crosses the planet position		2	4.8
4	The eUTC-line is parallelized with planet line		3	7.1
5	The eUTC-line is perpendicular with planet line		13	31.0

Table 8. The R8+ earthquake statistic for cRS schemes which are typical for recording signals from remote extrasolar sources.

	Remote Source cRS study cases, 28 pcs.	Quantity	
		pcs.	%
1	Triangle cRS scheme with resonance	23	82.1
2	Parallelism in the Triangle schemes	16	57.1
	The eUTC-line features in the RS schemes	**Quantity**	
		pcs.	**%**
1	eUTC-line, P-polarization	5	17.9
2	eUTC-line, S-polarization	3	10.7
	Total amount of eUTC-line events	23	82.1
	The Galaxy-Sun alignment in the cRS schemes	**Quantity**	
		pcs.	**%**
1	Mercury	6	21.4
2	Venus	4	14.3
3	Earth	1	3.6
4	Mars	1	3.6

Table 8 provides a summary of cRS cases. Note that it has been found that both the integer ratio in the distances between the planets and the planet parallelism increase this effect in cRS cases. The proportion of the triangular cRS schemes with resonance in the ratio of distances to planets is equal 82.1%. The planet parallelism quota in the cRS schemes is 57.1%. Note again that it is assumed that the integer ratio of the distance to the planet, as well as the parallelism of the planets, is an amplifying factor of gravitational interference. It is interesting to note another feature, namely the presence of Galaxy-Sun-planet alignment in cRS schemes, *i.e.* then the planets most often Venus and Mercury intersect the axis of the galaxy during an earthquake, which is the projection of the central Sun-galaxy line on the plane of the solar system. It is well-known that stars are compressing near a black hole and so the center of the galaxy can probably be a source of gravitational disturbance.

Therefore, according to the Archimedes Lever and Kepler conjunction principal, the Third Law of Motion must be changed by adding a few words to the end of the text of the law:

"*When one body exerts a force on a second body, the second body exerts a force equal in magnitude and opposite in direction to that of the first body in the absence of obstacles in the path between these bodies*"

(7)

Another interpretation was considered:

"*When in a vacuum or in a homogeneous and isotropic medium one body exerts a force on a second body, the second body exerts a force equal in magnitude and opposite in direction to that of the first*".

(7')

Finally note about relation this study with the previous our researches are presented in **Figure 15**. This scheme demonstrates severe, moderate and minor impacts to the Earth, which were investigated early in [71] [72], and by author in [3], and in this study.

It is important to note that recently new methods have been rapidly developing in astronomy. Thus, in 2007 it was recognized that in astronomy laser frequency combs (LFCs) may have some advantages, [73] [74]. Usually in astronomy, LFCs are called astronomical frequency combs ("*astro-combs*") instruments. These astro-combs have been optimized for astronomical applications to detect Earth-like exoplanets using radial velocity measurements, [75]-[81]. Currently, several important spectrographs in large observatories, such as the High Accuracy Radial velocity Planet Searcher (HARPS), the High Accuracy Radial velocity Planet Searcher for the Northern hemisphere (HARPS-N), the Solar Vacuum Tower Telescope (VTT) and the Fiber Optic Cassegrain Echelle Spectrograph (FOCES), are equipped with astro-combs, [80]. Discoveries of Earth-mass planets in the habitable zones were reported in [82] [83]. But astro-combs have been proposed as an improved calibration source, please see details in [75] [84] [85] [86] [87] [88].

Please note that the author has chosen a different, simpler method of searching for habitable star systems and in this study announces the imminent release of his new publication [89]. Combining efforts to search for habitable planets by various methods can be successful, which means that in the near future humanity will begin to explore star systems located at a distance of ~200 pc from our Solar System.

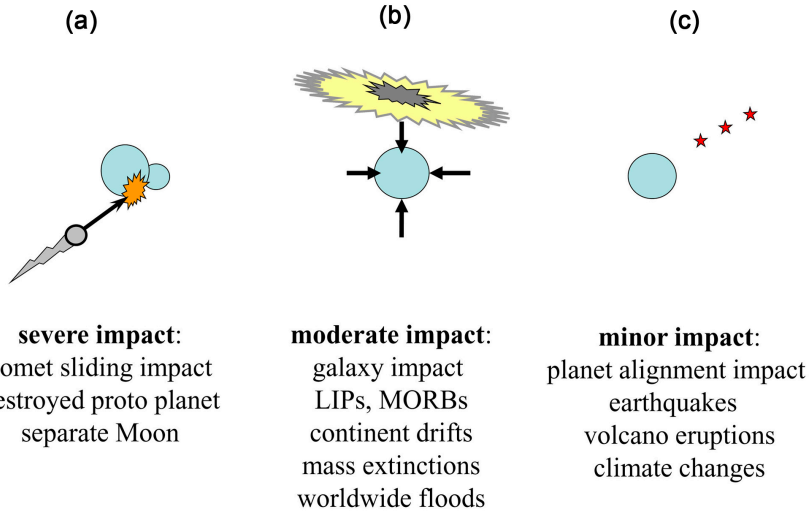

Figure 15. The scheme demonstrate severe (a), moderate (b) and minor (c) impacts to the Earth.

10. Discussion about Geometry and Gravitation

Many people believe that it was Albert Einstein who first established the connection between astronomy and geometry. This is not true. The connection between astronomy and geometry has been known in the Mediterranean since the time of Thales and Pythagoras. In the Ancient World, this statement was repeatedly mentioned by Plato, Socrates and Aristotle. The next significant milestone in the development was the establishment that inertial mass is equivalent to the gravitational mass. At the same time, it was shown that the inertial interaction is determined only by the geometry of the problem.

About 100 years ago, Albert Einstein suggested that gravity is determined by geometry. Albert Einstein was not very good at teaching; it is possible that when developing his theory of relativity, he did know about the works of Pythagoras, Archimedes, Plato, and Aristotle, nor about the later works of Kepler and Bode.

Now we known that gravity manifests itself in two hypostases, namely in the form of gravitational attraction and the force of inertia. The inertial interaction does not have a small gravitational coefficient γ, which is equal to 6.6743×10^{-11} $m^3 \cdot s^{-2} \cdot kg^{-1}$. Consequently, within the framework of a powerful inertial interaction, the planets and the Sun can have a significant impact on the Earth, including causing earthquakes and volcanic eruptions. This question is the object of this study, so we should pay attention to Einstein's axioms.

It was further noted that the equality of inertial and gravitational masses does not mean that these sets are the same. Schematically, the relations between the inertial and gravity sets are shown in Figure 16(a) and Figure 16(b). Thus, we bring the reader to the understanding that Albert Einstein unreasonably, in voluntaristic way, imposed the concept of the dominance of geometry over gravity.

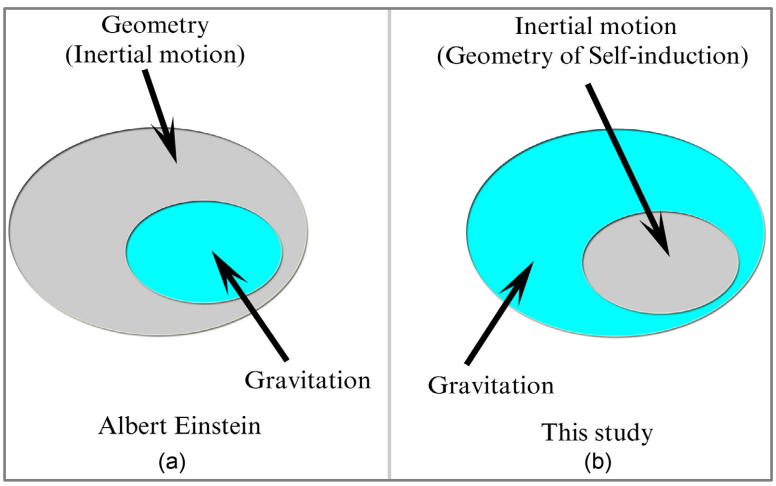

Figure 16. The potencies of the set of inertial motion (Geometry) and Gravitation by Albert Einstein (a) and in this study (b) are presented. In this study, inertial motion is a special case of general gravity, namely it is process of gravitational self-induction, which depends only on geometry. The process of self-induction is initialized by the shading of planets, that is, by Archimedes levers or Kepler conjunctions.

Table 9. Differences between the approaches of Albert Einstein and this study in the interpretation of the equivalence of inertial and gravitational masses.

Albert Einstein	This study
Comparison of capacity of sets:	
The geometric metric defines all the properties of gravity:	The inertia is a special case of gravity. Inertia is self-induction and is determined by the task of geometry:
$\text{Geometry} \supset \text{Inertia} \supseteq \text{Gravitation}$	$\text{Gravitation} \supset \text{Inertia}(\text{Geometry})$
The mass of a black hole in the center of the galaxy:	
The mass of the black hole is large:	The mass of a black hole is identically zero. Only the flow of matter through the cross section of a black hole is determined:
$M(\text{black hole}) \to \infty$	$M(\text{black hole}) \equiv 0$ $J(\text{black hole}) \sim const$
The amount of matter at the outer edge of the galaxy:	
At the outer boundary of the galaxy, matter is synthesized due to vacuum quantization:	Closing streams. The amount of matter that has passed through the center of the galaxy is approximately equal to the amount of matter at the outer edge of the galaxy:
$M(\text{outer galaxy border}) \approx 0$	$J(\text{outer galaxy border}) \approx J(\text{black hole})$
Motion of matter along the arm of galaxy:	
Translational motion of matter without rotation. The constancy of velocity is the result of the curvature of space.	Translational-screw motion, analogous to the Archimedes' screw. Please do not confuse the spirality of the galaxy with the spirality of the galaxy arm:
$S(\text{galaxy arm}) = 0$	$S(\text{galaxy arm}) \neq 0$
Generation of gravitational waves:	
This requires collisions of massive bodies, that is, gravitational waves can be generated at collisions of two massive black holes or large neutron stars:	The gravitational waves (vortex) can be generated by various objects, including small planets in the solar system:
$\sum M \sim M(\text{balck hole})$	$\sum M \sim M(\text{planet})$
The frequency of gravitational waves:	
The frequency is determined by the size of the generating system, thus the gravity waves have frequencies such as in the LIGO and VIRGO experiments:	The frequency is determined by the size of the generating system, thus the gravity waves have frequencies such as in the in future eLISA experiment:
$\lambda \sim L(\text{balck hole})$	$\lambda \sim L(\text{solar system})$

An alternative option, when inertial motion is a special case of gravity, is shown in Figure 15(b). In this case, inertial motion is a process of gravitational self-induction. The analogue of this process is well known in electrodynamics.

Note that the process of electrodynamics' self-induction is indeed determined only by the geometry of the task. At the same time, in electrodynamics, it does not occur to anyone to assert that a torus or a solenoid bends space and time. The difference in approaches between Albert Einstein's axiomatics and gravitational self-induction is presented in Table 9. Note that these differences are significant.

11. Conclusions

In this study, the geometry of the planets is studied, corresponding to the moment of strong earthquakes with a magnitude of more than 8 points on the Richter scale (R8+). A total of 92 cases of R8+ earthquakes that occurred between 1900 and 2011 were investigated. Three main planetary schemes have been identified, namely the generalized Archimedes lever (gAL) and Kepler conjunction (gKc) schemes, as well as a new catcher Remote Signal (cRS) triangles planetary geometry.

The total number of schemes, including schemes for capturing signals from remote sources, is surprisingly diverse, and cannot be reduced to the oldest schemes, such as the Archimedes lever and the Kepler conjunction. It was discovered 22 gAL, 42 gKc and 28 cRS geometries, which is 23.9%, 45.7%, and 30.4% of the total number of 92 studied cases, respectively.

It was further shown that a number of planetary geometry schemes correspond to previously known configurations. Namely, out of 92 studied earthquakes, 12 alignments of the Archimedes lever were found (L-scheme, Figure 2) and 9 Kepler conjunctions (Sun-L scheme, Figure 3). Moreover, it was shown that the gKc schemes (Sun-L and Sun-X, Figure 3) are dominant in all set of geometries schemes. At the same time, Jupiter dominates in these gKc schemes; Jupiter participates in 54.8% of cases, Venus in 47.6%, and Mercury in 38.1%. That is, it is really possible to talk about some "*Jupiter effect*", see additionally [3] [7] [10] [64] and others.

Further, it was noted for the first time that the 30.4% of the total number of cases studied correspond to resonant triangular structures called in this study as catcher Remote Signal (cRS) resonance. However, this work does not answer the question whether the recorded signals were generated in the solar system itself or came from outside.

Also in this work, the angles of rotation of the planet, measured in the planetary plane at the time of the earthquake, are investigated. It was found that the planetary geometries of some earthquakes are absolutely identical, which specifies in universality of the earthquake triggered mechanism. It is further shown that the triggered effect does not depend on the distance between the planets and the mass of the planets, so it was identified as an inertial gravitational interaction. The effect increases with increasing multiplicity of the ratio of distances between the planets, as well as with pairwise parallelism of the planetary geometries, which probably indicates the wave nature of inertial effects in the schemes

X, Sun-X and cRS.

As part of the consideration of the Aristotle relationship between nature, geometry and astronomy, critical remarks concerning Einstein's axiomatics are written. We push the reader to understand that Albert Einstein imposed the concept of the dominance of geometry over gravity in an unreasonable, voluntaristic way. In this study, it is assumed that inertia is a special case of gravity, namely gravitational self-induction, which really depends, like any self-induction, only on the geometry of the task.

Acknowledgements

The author gratefully acknowledges colleagues and my wife for suggesting the topic of this paper and for the very thorough revision of the manuscript.

Conflicts of Interest

The author declares no conflicts of interest regarding the publication of this paper.

References

[1] Safronov, A.N. (2016) Antikythera Mechanism and the Ancient World. *Journal of Archaeology*, **2016**, Article ID: 8760513. https://doi.org/10.1155/2016/8760513

[2] Safronov, A.N. (2020) The Archimedes' Lever and Vesuvius Eruption A.D. 79. *Journal of Anthropological and Archaeological Sciences*, **1**, 98-115. https://doi.org/10.32474/JAAS.2020.01.000119

[3] Safronov, A.N. (2022) New Theory of Effusive and Explosive Volcanic Eruptions. *International Journal of Geosciences*, **13**, 115-137. https://doi.org/10.4236/ijg.2022.132007

[4] Tomaschek, R. (1959) Great Earthquakes and the Astronomical Positions of Uranus. *Nature*, **184**, 177-178. https://doi.org/10.1038/184177a0

[5] Burr, E.J. (1960) Earthquakes and Uranus: Misuse of a Statistical Test of Significance. *Nature*, **186**, 336-337. https://doi.org/10.1038/186336b0

[6] Gribbin, J. (1973) Planetary Alignments, Solar Activity and Climatic Change. *Nature*, **246**, 453-454. https://doi.org/10.1038/246453a0

[7] Gribben, J.R. and Plagemann, S.H. (1974) The Jupiter Effect: The Planets as Triggers of Devastating Earthquakes. Walker, New York.

[8] Gribben, J. (1975) Predicting Earthquakes. *Physics Today*, **28**, 13-15. https://doi.org/10.1063/1.2998912

[9] Gribben, J. and Plagemann, S. (1975) Response to Meeus. *Icarus*, **26**, 268-269. https://doi.org/10.1016/0019-1035(75)90087-1

[10] Meeus, J. (1975) Comments on the Jupiter Effect. *Icarus*, **26**, 257-267. https://doi.org/10.1016/0019-1035(75)90086-X

[11] Meeus, J. (1975) Reply to Grihben and Plagemann. *Icarus*, **26**, 270. https://doi.org/10.1016/0019-1035(75)90088-3

[12] Gribben, J. (1976) The Author Comments. *Physics Today*, **29**, 11-13. https://doi.org/10.1063/1.3023411

[13] Bolt, B.A. and Wang, C.-Y. (1975) The Present Status of Earthquake Prediction.

CRC Critical Reviews in Solid State Sciences, **5**, 125-151.
https://doi.org/10.1080/10408437508243477

[14] Ip, W.H. (1976) Chinese Records on the Correlation of Heliocentric Planetary Alignments and Earthquakes Activities. *Icarus*, **29**, 435-436.
https://doi.org/10.1016/0019-1035(76)90144-5

[15] Hughes, D.W. (1977) Planetary Alignments Don't Cause Earthquakes. *Nature*, **265**, 13. https://doi.org/10.1038/265013a0

[16] Geller, R.J. (1997) Earthquake Prediction: A Critical Review. *Geophysical Journal International*, **131**, 425-450. https://doi.org/10.1111/j.1365-246X.1997.tb06588.x

[17] Geller, R.J. (1997) Earthquakes Cannot Be Predicted. *Science*, **275**, 1616-1610.
https://doi.org/10.1126/science.275.5306.1616

[18] Omerbashich, M. (2012) Astronomical Alignments as the Cause of ~M6+ Seismicity. Cornell University Library. arXiv: 1104.2036v1107, arxiv.org/abs/1104.2036

[19] Mörner, N.-A., Tattersall, R., Solheim, J.-E., Charvatova, I., Scafetta, N., Jelbring, H., Wilson, I.R., Salvador, R., Willson, R.C., Hejda, P., Soon, W., Velasco Herrera, V.M., Humlum, O., Archibald, D., Yndestad, H., Easterbrook, D., Casey, J., Gregori, G. and Henriksson, G. (2013) General Conclusions Regarding the Planetary-Solar-Terrestrial Interaction. *Pattern Recognition in Physics*, **1**, 205-206.
https://doi.org/10.5194/prp-1-205-2013

[20] Scafetta, N. (2014) The Complex Planetary Synchronization Structure of the Solar System. *Pattern Recognition in Physics*, **2**, 1-19.
https://doi.org/10.5194/prp-2-1-2014

[21] Scafetta, N. and Mazzarella, A. (2015) Spectral Coherence between Climate Oscillations and the M > 7 Earthquake Historical Worldwide Record. *Natural Hazards*, **76**, 1807-1829. https://doi.org/10.1007/s11069-014-1571-z

[22] Marilia, H. and Azevedo, A. (2017) Possible Connections between X-Solar Flares and Worldwide Variation in Seismicity Enhancement. *Natural Science*, **9**, 457-476.
https://doi.org/10.4236/ns.2017.912042

[23] Hagen, M. and Azevedo, A. (2019) Sun-Moon-Earth Interactions with Larger Earthquakes Worldwide Connections. *Open Journal of Earthquake Research*, **8**, 267-298. https://doi.org/10.4236/ojer.2019.84016

[24] Awadh, S.M. (2021) Solar System Planetary Alignment Triggers Tides and Earthquakes. *Journal of Coastal Conservation*, **25**, Article No. 30.
https://doi.org/10.1007/s11852-021-00822-7

[25] Bollinger, C.J. (1952) A 44.77 Year Jupiter-Venus-Earth Configuration Sun-Tide Period in Solar-Climatic Cycles. *Proceedings of the Oklahoma Academy of Science*, **33**, 307-311.

[26] Simpson, J.F. (1968) Solar Activity as a Triggering Mechanism for Earthquake. *Earth and Planetary Science Letters*, **3**, 417-425.
https://doi.org/10.1016/0012-821X(67)90071-4

[27] Gribben, J. (1971) Relation of Sunspot and Earthquake Activity. *Science*, **173**, 558.
https://doi.org/10.1126/science.173.3996.558.b

[28] Wood, K. (1972) Sunspots and Planets. *Nature*, **240**, 91-93.
https://doi.org/10.1038/240091a0

[29] Anderson, D.L. (1974) Earthquakes and the Rotation of the Earth. *Science*, **186**, 49-50. https://doi.org/10.1126/science.186.4158.49

[30] Condon, J.J. and Schmidt, R.R. (1975) Planetary Tides and the Sunspot Cycles. *Solar Physics*, **42**, 529-532. https://doi.org/10.1007/BF00149930

[31] Gu, Z.-N. (1995) The Study of Excitation of the Earthquake to Earth's Rotation. *Earth, Moon and Planets*, **74**, 35-47. https://doi.org/10.1007/BF00118720

[32] Zharov, V.E. (1996) Connection of the Earth's Rotation with the Atmospheric Angular Momentum and the Strongest Earthquake. *Astronomical and Astrophysical Transactions*, **9**, 317-327. https://doi.org/10.1080/10556799608208230

[33] Soldati, G. and Spada, G. (1999) Large Earthquakes and Earth Rotation: The Role of Mantle Relaxation. *Geophysical Research Letters*, **26**, 911-914. https://doi.org/10.1029/1999GL900144

[34] Han, Y., Guo, Z., Wu, J. and Ma, L. (2004) Possible Triggering of Solar Activity to Big Earthquakes (M > 8) in Faults with Near West-East Strike in China. *Science in China Series G: Physics, Mechanics and Astronomy*, **47**, 173-181. https://doi.org/10.1360/03yw0103

[35] Li, Y. (2006) An Examination of the Correlation between Earthquake, Positions of Solar System Bodies and Solid Tide. *Science in China Series G*, **49**, 367-376. https://doi.org/10.1007/s11433-006-0367-x

[36] Hung, C.-C. (2007) Apparent Relations between Solar Activity and Solar Tides Caused by the Planets. NASA/TM-2007-214817, 1.

[37] Odintsov, S.D., Ivanov-Kholodnyi, G.S. and Georgieva, K. (2007) Solar Activity and Global Seismicity of the Earth. *Bulletin of the Russian Academy of Sciences: Physics*, **71**, 593-595. https://doi.org/10.3103/S1062873807040466

[38] Scafetta, N. (2010) Empirical Evidence for a Celestial Origin of the Climate Oscillations and Its Implications. *Journal of Atmospheric and Solar-Terrestrial Physics*, **72**, 951-970. https://doi.org/10.1016/j.jastp.2010.04.015

[39] Tavares, M. and Azevedo, A. (2011) Influences of Solar Cycles on Earthquakes. *Natural Science*, **3**, 436-443. https://doi.org/10.4236/ns.2011.36060

[40] Abreu, J.A., Beer, J., Ferriz-Mas, A., McCracken, K.G. and Steinhilber, F. (2012) Is There a Planetary Influence on Solar Activity? *Astronomy & Astrophysics*, **548**, Article No. A88. https://doi.org/10.1051/0004-6361/201219997

[41] Okhlopkov, V.P. (2014) The 11-Year Cycle of Solar Activity and Configurations of the Planets. *Moscow University Physics Bulletin*, **69**, 257-262. https://doi.org/10.3103/S0027134914030126

[42] Scafetta, N. (2014) Discussion on the Spectral Coherence between Planetary, Solar and Climate Oscillations: A Reply to Some Critiques. *Astrophysics and Space Science*, **354**, 275-299. https://doi.org/10.1007/s10509-014-2111-8

[43] Stefani, F., Giesecke, A., Weber, N. and Weier, T. (2016) Synchronized Helicity Oscillations: A Link between Planetary Tides and the Solar Cycle? *Solar Physics*, **291**, 2197-2212. https://doi.org/10.1007/s11207-016-0968-0

[44] Stefani, F., Giesecke, A. and Weier, T. (2019) A Model of a Tidally Synchronized Solar Dynamo. *Solar Physics*, **294**, Article No. 60. https://doi.org/10.1007/s11207-019-1447-1

[45] Marchitelli, V., Harabaglia, P., Troise, C. and de Natale, G. (2020) On the Correlation between Solar Activity and Large Earthquakes Worldwide. *Scientific Reports*, **10**, Article ID: 11495. https://doi.org/10.1038/s41598-020-67860-3

[46] Dermott, S.F. (1973) Bode's Law and the Resonant Structure of the Solar System. *Nature Physical Science*, **244**, 18-21. https://doi.org/10.1038/physci244018a0

[47] Lecar, M. (1973) Bode's Law. *Nature*, **242**, 318-319. https://doi.org/10.1038/242318a0

[48] Nieto, M.M. (1975) The Titius-Bode Law and the Possibility of Recent Large-Scale

Evolution in the Solar System. *Icarus*, **25**, 171-174. https://doi.org/10.1016/0019-1035(75)90196-7

[49] Ovenden, M.W. (1972) Physical Sciences: Bode's Law and the Missing Planet. *Nature*, **239**, 508-509. https://doi.org/10.1038/239508a0

[50] Bass, R.W. and Del Popolo, A. (2005) Dynamical Derivation of Bode's Law. *International Journal of Modern Physics D*, **14**, 153-169. https://doi.org/10.1142/S0218271805006195

[51] Bovaird, T. and Lineweaver, C.H. (2013) Exoplanet Predictions Based on the Generalised Titius-Bode Relation. *Monthly Notices of the Royal Astronomical Society*, **435**, 1126-1138. https://doi.org/10.1093/mnras/stt1357

[52] Huang, C.X. and Bakos, G.A. (2014) Testing the Titius-Bode Law Predictions for Kepler Multi-Planet Systems. *Monthly Notices of the Royal Astronomical Society*, **442**, 674-681. https://doi.org/10.1093/mnras/stu906

[53] Amaro-Seoane, P., Aoudia, S., Babak, S., Binétruy, P., Berti, E., Bohé, A., Caprini, C., Colpi, M., Cornish, N.J., Danzmann, K., Dufaux, J.-F., Gair, J., Jennrich, O., Jetzer, P., Klein, A., Lang, R.N., Lobo, A., Littenberg, T., McWilliams, S.T., Nelemans, G., Petiteau, A., Porter, E.K., Schutz, B.F., Sesana, A., Stebbins, R., Sumner, T., Vallisneri, M., Vitale, S., Volonteri, M. and Ward, H. (2012) Low-Frequency Gravitational-Wave Science with eLISA/NGO. *Classical and Quantum Gravity*, **29**, Article ID: 124016. https://doi.org/10.1088/0264-9381/29/12/124016

[54] Datasets (2021) EM-DAT—CRED International Disaster Database. Centre for Research on the Epidemiology of Disasters (CRED), Brussels. https://public.emdat.be

[55] CRED Report 2021 (2022) Disasters in Numbers. CRED, Brussels. https://cred.be/sites/default/files/2021_EMDAT_report.pdf

[56] Guha-Sapir, D., D'Aoust, O., Vos, F. and Hoyois, P. (2013) The Frequency and Impact of Natural Disasters. Oxford University Press, London. https://doi.org/10.1093/acprof:oso/9780199841936.003.0002

[57] Guha-Sapir, D., Hoyois, P., Wallemacq, P. and Below, R. (2016) Annual Disaster Statistical Review 2016: The Numbers and Trends. Center for Research on the Epidemiology of Disasters (CRED), Brussels. https://reliefweb.int/attachments/c5755216-3feb-3871-b5c6-63d52481ab76/adsr_2016.pdf

[58] Chaudhary, M.T. and Piracha, A. (2021) Natural Disasters—Origins, Impacts, Management. *MDPI Encyclopedia*, **1**, 1101-1131. https://doi.org/10.3390/encyclopedia1040084

[59] Datasets: "Magnitude 8 and Greater Earthquakes Since 1900", USGS, Earthquake Hazards Program, "Magnitude 8 and Greater Earthquakes Since 1900". https://web.archive.org/web/20091112231732/http://earthquake.usgs.gov/earthquakes/eqarchives/year/mag8/magnitude8_1900_date.php

[60] National Geophysical Data Center/World Data Service (NGDC/WDS): NCEI/WDS Global Significant Earthquake Database. NOAA National Centers for Environmental Information. https://www.ncei.noaa.gov/access/metadata/landing-page/bin/iso?id=gov.noaa.ngdc.mgg.hazards:G012153

[61] Datasets: "Historic World Earthquakes", USGS, Earthquake Hazards Program, "Historic World Earthquakes".

[62] Osamu, A. and Ron, B. Osamu Ajiki 1996, Ron Baalke, 2000-2001, "OrbitViewer Applet". http://www.astroarts.jp/products/orbitviewer/OrbitViewer-1.3.tar.gz

[63] JPL Small-Body Database Browser NASA, California Institute of Technology, Jet Propulsion Laboratory (JPL), JPL Small-Body Database Browser, Orbit Diagram (for 1P/Halley). https://ssd.jpl.nasa.gov/tools/sbdb_lookup.html#/?des=1P

[64] Wilson, I.R.G. (2013) The Venus-Earth-Jupiter Spin-Orbit Coupling Model. *Pattern Recognition in Physics*, **1**, 147-158. https://doi.org/10.5194/prp-1-147-2013

[65] eLISA Consortium, Amaro Seoane, P., Aoudia, S., Audley, H., Auger, G., Babak, S., Baker, J., Barausse, E., Barke, S., Bassan, M., *et al.* (2013) The Gravitational Universe. arXiv e-prints, arXiv:1305.5720

[66] Wang, G. and Ni, W.-T. (2013) Numerical Simulation of Time Delay Interferometry for eLISA/NGO. *Classical and Quantum Gravity*, **30**, Article ID: 065011. https://doi.org/10.1088/0264-9381/30/6/065011

[67] Cornish, N. and Robson, T. (2017) Galactic Binary Science with the New LISA Design. *Journal of Physics*: *Conference Series*, **840**, Article ID: 012024. https://doi.org/10.1088/1742-6596/840/1/012024

[68] Amaro-Seoane, P., Audley, H., Babak, S., Baker, J., Barausse, E., Bender, P., Berti, E., Binetruy, P., Born, M. and Bortoluzzi, D. (2017) Laser Interferometer Space Antenna. arXiv e-prints, arXiv:1702.00786

[69] Baker, J., Haiman, Z., Rossi, E.M., Berger, E., Brandt, N., Breedt, E., Breivik, K., Charisi, M., Derdzinski, A. and D'Orazio, D.J. (2019) Multimessenger Science Opportunities with mHz Gravitational Waves. *Bulletin of the American Astronomical Society* (*BAAS*), **51**, 123.

[70] eLISA Consortium (2020) The Laser Interferometer Space Antenna. Unveiling the Millihertz Gravitational Wave Sky.

[71] Safronov, A.N. (2016) The Basic Principles of Creation of Habitable Planets around Stars in the Milky Way Galaxy. *International Journal of Astronomy and Astrophysics*, **6**, 512-554. https://doi.org/10.4236/ijaa.2016.64039

[72] Safronov, A.N. (2020) A New View of the Mass Extinctions and the Worldwide Floods. *International Journal of Geosciences*, **11**, 251-287. https://doi.org/10.4236/ijg.2020.114014

[73] Murphy, M.T., Udem, T., Holzwarth, R., Sizmann, A., Pasquini, L., Araujo-Hauck, C., Dekker, H., d'Odorico, S., Fischer, M., Hänsch, T.W. and Manescau, A. (2007) High-Precision Wavelength Calibration of Astronomical Spectrographs with Laser Frequency Combs. *Monthly Notices of the Royal Astronomical Society*, **380**, 839-847. https://doi.org/10.1111/j.1365-2966.2007.12147.x

[74] Steinmetz, T., Wilken, T., Araujo-Hauck, C., Holzwarth, R., Hansch, T.W., Pasquini, L., Manescau, A., D'Odorico, S., Murphy, M.T., Kentischer, T., Schmidt, W. and Udem, T. (2008) Laser Frequency Combs for Astronomical Observations. *Science*, **321**, 1335-1337. https://doi.org/10.1126/science.1161030

[75] Wilken, T., Curto, G.L., Probst, R.A., Steinmetz, T., Manescau, A., Pasquini, L., Gonzalez Hernandez, J.I., Rebolo, R., Hansch, T.W., Udem, T. and Holzwarth, R. (2012) A Spectrograph for Exoplanet Observations Calibrated at the Centimetre-per-Second Level. *Nature*, **485**, 611-614. https://doi.org/10.1038/nature11092

[76] Ycas, G.G., Quinlan, F., Diddams, S.A., Osterman, S., Mahadevan, S., Redman, S., *et al.* (2012) Demonstration of On-Sky Calibration of Astronomical Spectra Using a 25 GHz Near-IR Laser Frequency Comb. *Optics Express*, **20**, 6631-6643. https://doi.org/10.1364/OE.20.006631

[77] Li, C., Glenday, A.G., Chang, G., Chen, L., Furesz, G., Langellier, N., Zibrov, A., Kärtner, F., Phillips, D.F., Sasselov, D., Szentgyorgyi, A. and Walsworth, R.L. (2014)

A Green Astro-Comb for Earth-Like Exoplanet Searches. *Frontiers in Optics* 2014 *Tucson*, Arizona, 19-23 October 2014, FW5D.2. https://doi.org/10.1364/FIO.2014.FW5D.2

[78] Glenday, A.G., Li, C.-H., Langellier, N., Chang, G., Chen, L.-J., Furesz, G., Zibrov, A.A., Kärtner, F., Phillips, D.F., Sasselov, D., Szentgyorgyi, A. and Walsworth, R.L. (2015) Operation of a Broadband Visible-Wavelength Astro-Comb with a High-Resolution Astrophysical Spectrograph. *Optica*, **2**, 250-254. https://doi.org/10.1364/OPTICA.2.000250

[79] Yi, X., Vahala, K., Li, J., Diddams, S., Ycas, G., Plavchan, P., *et al.* (2016) Demonstration of a Near-IR Line-Referenced Electro-Optical Laser Frequency Comb for Precision Radial Velocity Measurements in Astronomy. *Nature Communications*, **7**, Article No. 10436. https://doi.org/10.1038/ncomms10436

[80] Probst, R.A., Steinmetz, T., Wu, Y., Grupp, F., Udem, T. and Holzwarth, R. (2017) A Compact Echelle Spectrograph for Characterization of Astro-Combs. *Applied Physics B*, **123**, Article No. 76. https://doi.org/10.1007/s00340-016-6628-0

[81] Suh, M.-G., Yi, X., Lai, Y.-H., Leifer, S., Grudinin, I.S., Vasisht, G., *et al.* (2018) Searching for Exoplanets Using a Microresonator Astrocomb. *Nature Photonics*, **13**, 25-30. https://doi.org/10.1038/s41566-018-0312-3

[82] Anglada-Escudé, G., Amado, P.J., Barnes, J., Berdiñas, Z.M., Butler, R.P., Coleman, G.A.L., de la Cueva, I., Dreizler, S., Endl, M., Giesers, B., Jeffers, S.V., Jenkins, J.S., Jones, H.R.A., Kiraga, M., Kürster, M., López-González, M.J., Marvin, C.J., Morales, N., Morin, J., Nelson, R.P., Ortiz, J.L., Ofir, A., Paardekooper, S.-J., Reiners, A., Rodríguez, E., Rodríguez-López, C., Sarmiento, L.F., Strachan, J.P., Tsapras, Y., Tuomi, M. and Zechmeister, M. (2016) A Terrestrial Planet Candidate in a Temperate Orbit around Proxima Centauri. *Nature*, **536**, 437-440. https://doi.org/10.1038/nature19106

[83] Gillon, M., Triaud, A.H.M.J., Demory, B.-O., Jehin, E., Agol, E., Deck, K.M., Lederer, S.M., de Wit, J., Burdanov, A., Ingalls, J.G., Bolmont, E., Leconte, J., Raymond, S.N., Selsis, F., Turbet, M., Barkaoui, K., Burgasser, A., Burleigh, M.R., Carey, S.J., Chaushev, A., Copperwheat, C.M., Delrez, L., Fernandes, C.S., Holdsworth, D.L., Kotze, E.J., Van Grootel, V., Almleaky, Y., Benkhaldoun, Z., Magain, P. and Queloz, D. (2017) Seven Temperate Terrestrial Planets around the Nearby Ultracool Dwarf Star TRAPPIST-1. *Nature*, **542**, 456-460. https://doi.org/10.1038/nature21360

[84] Molaro, P., Esposito, M., Monai, S., Lo Curto, G., González Hernández, J.I., Hänsch, T.W., Holzwarth, R., Manescau, A., Pasquini, L., Probst, R.A., Rebolo, R., Steinmetz, T., Udem, T. and Wilken, T. (2013) A Frequency Comb Calibrated Solar Atlas. *Astronomy & Astrophysics*, **560**, Article No. A61. https://doi.org/10.1051/0004-6361/201322324

[85] Zou, P., Steinmetz, T., Falkenburger, A., Wu, Y.J., Fu, L.T., Mei, M. and Holzwarth, R. (2016) Broadband Frequency Comb for Calibration of Astronomical Spectrographs. *Journal of Applied Mathematics and Physics*, **4**, 202-205. https://doi.org/10.4236/jamp.2016.42025

[86] Fischer, D.A., Anglada-Escude, G., Arriagada, P., Baluev, R.V., Bean, J.L., Bouchy, F., Buchhave, L.A., Carroll, T., Chakraborty, A., Crepp, J.R., Dawson, R.I., Diddams, S.A., Dumusque, X., Eastman, J.D., Endl, M., Figueira, P.F., Eric B., Foreman-Mackey, D., Fournier, P., Furesz, G., Gaudi, B.S., Gregory, P.C., Grundahl, F., Hatzes, A.P., Hebrard, G., Herrero, E., Hogg, D.W., Howard, A.W., Johnson, J.A., Jorden, P., Jurgenson, C.A., Latham, D.W., Laughlin, G., Loredo, T.J., Lovis, C., Mahadevan, S., McCracken, T.M., Pepe, F., Perez, M., Phillips, D.F., Plavchan, P.P., Prato, L., Quirrenbach, A., Reiners, A., Robertson, P., Santos, N.C., Sawyer, D., Se-

gransan, D., Sozzetti, A., Steinmetz, T., Szentgyorgyi, A.U., Udry, S., Valenti, J.A., Wang, S.X., Wittenmyer, R.A. and Wright, J.T. (2016) State of the Field: Extreme Precision Radial Velocities. *Publications of the Astronomical Society of the Pacific*, **128**, Article ID: 066001. https://doi.org/10.1088/1538-3873/128/964/066001

[87] Boggio, C.J.M., Fremberg, T., Bodenmuller, D., Sandin, C., Zajnulina, M., Kelz, A., Giannone, D., Rutowska, M., Moralejo, B., Roth, M.M., Wysmolek, M. and Sayinc, H. (2018) Wavelength Calibration with PMAS at 3.5 m Calar Alto Telescope Using a Tunable Astro-Comb. *Optics Communications*, **415**, 186-193. https://doi.org/10.1016/j.optcom.2018.01.007

[88] Probst, R.A., Milaković, D., Toledo-Padron, B., Lo Curto, G., Avila, G., Brucalassi, A., Canto Martins, B.L., de Castro Leão, I., Esposito, M., González Hernández, J.I., Grupp, F., Hänsch, T.W., Kellermann, H., Kerber, F., Mandel, O., Manescau, A., Pozna, E., Rebolo, R., de Medeiros, J.R., Steinmetz, T., Suárez Mascareño, A., Udem, T., Urrutia, J., Wu, Y., Pasquini, L. and Holzwarth, R. (2020) A Crucial Test for Astronomical Spectrograph Calibration with Frequency Combs. *Nature Astronomy*, **4**, 603-608. https://doi.org/10.1038/s41550-020-1010-x

[89] Safronov, A.N. (2022) Life Origin in the Milky Way Galaxy: Scanning for Habitable Stellar Systems on Behalf of Future Space Missions. (In press)

Supplementary Materials

The supporting materials, included 46 Figures S1-S46, could be requested from the author or can be obtained by Research Gate System. The planetary alignments for these Figures are described above in Tables 3-6 in the text of the manuscript.